Experimental analysis of analytical wake models for wind turbines

Master Thesis

Luis García Salgado

Aalborg University
Energy Department

Front page picture: Horns Rev offshore wind farm west of Denmark. Credit: Vattenfall

AALBORG UNIVERSITY

Energy Engineering
Aalborg University
http://www.aau.dk

Title:
Experimental analysis of analytical wake models for wind turbines

Theme:
Scientific Theme

Project Period:
Spring Semester 2017

Project Group:
OES10-4

Participant:
Luis García Salgado

Supervisors:
Mohsen Soltani

Copies: 1

Page Numbers: 47

Date of Completion:
May 27, 2017

Abstract:

In a cluster of wind turbines, the interference between wind turbines affect negatively. Upstream wind turbines generate wakes where the velocity is reduced and the turbulence increased. A reduced power leads in lower efficiency and the high turbulence intensity generate fluctuating loads that creates fatigue problems. As a result, a fully understand of the wake is needed in order to improve the wind turbines arrays.
Five models are investigated to predict the wake velocity decay and width development. Also, three models to describe the turbulence intensity are studied. Measurements from wind tunnel experiments are used to validate the models. The evaluation of the results shows that models can describe the behaviour of the wake characteristics fairly well. The prediction of the velocity deficit as well as the width in the wake behind the turbine, are found to deviate with around only 3% from the results, when the best analytical model is applied. More spread results are obtained regarding the turbulence intensity predictions, however, accurate results can be achieved. Thus, it can be concluded that analytical wake models are well suited to estimate the velocity deficit, width development and the turbulence intensity in the far wake of a wind turbine.

[This page intentionally left blank]

Contents

List of Figures

List of Tables

Preface

This thesis concludes my Master of Science in Engineering, Sustainable Energy Engineering, Offshore Energy Systems at Aalborg University.

Aalborg University, May 27, 2017

Luis Garcia Salgado
<lgarci15@student.aau.dk>

Chapter 1

Introduction

The amount of the total energy produced worldwide by harnessing wind energy has been increased over the last decades [1]. Wind energy is used as it shows numerous benefits such as it is a non polluted renewable source of energy, domestic source of energy, inexhaustible and cost- effective. Also, governments promote it with ambitious goals, such as the European Union which aims to reach a 20% of the share of energy from renewable sources in overall Community energy consumption by 2020 [2]. To achieve all the energy requirements, increasing the wind farms is needed in size and in number. As a result, wind farms are getting bigger and bigger, however, the overall efficiency cannot be calculated as the total sum of each wind turbine as there is an interaction between them.

This interaction, called wake, occurs between wind turbines which are in line with the wind direction. The first row of wind turbine creates the wake and affect the downstream turbines [3]. The wake depends on different parameters, which are explained further in section 1.1. The wake creates negative consequences both in the overall efficiency, as there is a decrease on the energy production due to the reduction of the wind velocity [4] and in the wind turbine itself, as the rise of the turbulence levels increase substantially the fluctuating loads, which lead into an increase of the fatigue rotor loads, decreasing the lifespan of the wind turbine [5].

To avoid the effects of the wake, typically the wind turbines are sited around 10 diameters (D) between each other in the main direction of the wind [6], however, due to optimization costs, this distance is reduced. Closer turbines means less space of land or sea and cheaper installation costs, cabling for instance as the required distance is shorter.

1.1 Wake

A wake is formed behind a solid body which has been placed in a flow fluid stream. The drag created during the extraction of the energy, generates a loss of momentum in the fluid, that it is translated into a decrease of the velocity of the flow just behind the wind turbine, compared with the velocity in the free flow stream [7]. The reduction of the wind speed depends mainly of three factors; the distribution of wind speed and direction; characteristics of the wind turbine and the characteristic of the wake [8].

The wake recovers its normal velocity some distance downstream the wind turbine, as the stream flow that was not affected remains with the same velocity and energize the flow that was reduced by the turbine. At the same time the width of the wake expands as the distance downstream increased. This recovery distance depends on several factors [9]:

- Turbulence levels in the atmosphere
- Surface constrain effects
- Wind shear effects
- Topographic and structural effects

In this project, there are three main characteristic that are used to describe the wake:

- *Velocity deficit (u_1)*: this parameter describes how the velocity is affected by the wind turbine. It is defined as the difference between the free stream flow velocity (U_∞) and the velocity at the measured point (U)

$$u_1 = U_\infty - U \tag{1.1}$$

- *Width development (b)*: it describes how wide the wake is at a certain downstream distance from the wind turbine.

$$b = f(x) \tag{1.2}$$

- *Turbulence intensity (TI)*:it is defined as the velocity fluctuation over the mean velocity.

$$TI = \frac{u}{u'} \tag{1.3}$$

1.2 Wake areas

During the literature research, among others [3], [6], [10], it is found that clearly can be distinguish two region in which the wake can be divided into, near wake and far wake. Both regions can be observed in figure 1.1. The border between both region is quite vague and is not easy to define. In some publications it is considered that the near wake is over when the shear layer becomes thick and it reaches the wake axis [3].

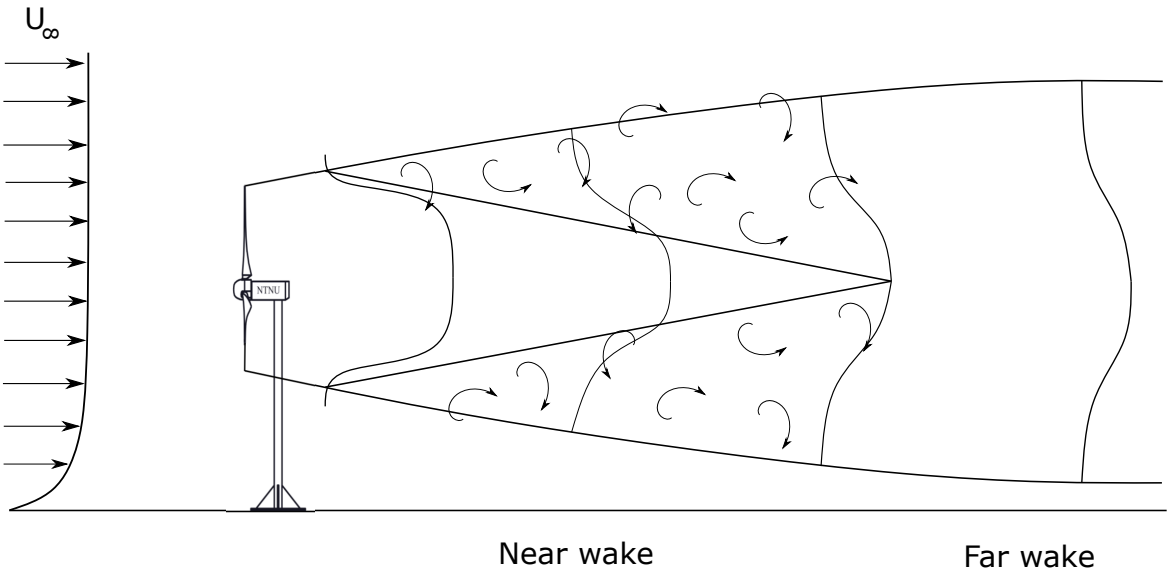

Figure 1.1: Diagram of the different regions of the wake behind a wind turbine

1.2.1 Near wake

It is a difficult area to model due the complex physics that are occurring inside. The maximum velocity deficit is situated in this region, usually after 1-2 D [11]. The expansion length is around 1 D. It is estimate that the wake is fully expanded between 2.25 - 5 D [10], that is when the shear layer becomes thick and it reaches the wake axis it is considered the end of the near wake.

1.2.2 Far wake

The far wake region is where this study is performed. It is located downstream of the near wake previously explained. In this area, the wake is completely developed, where is considered that the both profiles velocity deficit and turbulent intensity are axis-symmetric and have self-similar distribution in the cross-section of the wake [3].

1.3 Problem formulation

It is interest to know the wake characteristics in wind farms in order to predict power losses and mechanical loads. The main objective of this project is to study if the analytical models are able to estimate the characteristics of the wake in order to being able to control a wind farm and increase the overall efficiency and reduced the fatigue loads of the wind farm.

Analytical models were chosen as they are fast and easy to implement compared with numerical models, which required much more time to perform the calculations. In order to validate the models, the results of them were compared with experimental data from a measurement campaign in a wind tunnel.

1.4 Thesis organization

This thesis is organized as follows:

- **Chapter 2** describes the models that are used in this study to analyzed the behaviour of the wake including the velocity decay, width development and turbulence intensity.
- **Chapter 3** gives a description of the experimental setup and the instrumentation used to carry on the experiments. Also, an explanation of the procedures used during the measurement campaign.
- **Chapter 4** presents the results from the different measurements campaigns performed to analyzed the the different characteristics of the wake.
- **Chapter 5** discuss the different model agreement with the data as well the influence of the studied parameters including the ambient turbulence intensity.
- **Chapter 6** include the final conclusions for the project.
- **Chapter 7** exhibit the suggested further research of the presented project.

Chapter 2

Wake modelling

In this chapter, different wake models to estimate the development of important parameters in the wake such as velocity decay, width of the wake and turbulence intensity are explained.

2.1 Velocity decay and width development

The models analyzed in this study to describe the velocity decay and the width development are kinematic models and engineering expression or analytical expressions. The kinematic expressions are based on momentum theory, energy equation conservation of mass and self-similar velocity deficit profiles. Whereas, the analytical expression models are based in regressions or correlation that were found in experiments and they are not theoretical based [3].

2.1.1 Schlichting Model

A model developed by H. Schlichting in the Boundary Layer Theory [7], is studied. On it, the width development and the velocity decay of the wake behind blunt bodies are described with simple analytical expressions. Therefore, to use this model, it is necessary to prove that the wake of a wind turbines behaves as the wake create by a blunt bodies in the far wake.

The studied model is derived from the boundary layer equation for incompressible

flow and constrained to free turbulent flows, where the laminar friction can be neglected due to a much higher turbulent friction [7]. It is also assumed that the pressure across the wake remains constant. Due to this assumption, the model is only valid from a certain distance downstream the body.

The results that describe the width and the velocity decay from the derivation are the analytical expressions shown in table 2.1.

Type of flow	Width development	Velocity decay
Two-dimensional wake	$x^{1/2}$	$x^{-1/2}$
Circular wake	$x^{1/3}$	$x^{-2/3}$

Table 2.1: Analytical expressions for width and velocity decay in terms of downstream distance (x) from the blunt body [7].

In this study, the expressions that are used are the corresponding to the circular wake. To be able to compare the results of the model with different geometries, the expressions for b and u_1, which are described in table 2.1 are normalized. Consequently, b is normalized with the diameter of the rotor, giving the expression:

$$\frac{b}{D} = C_b \cdot \left(\frac{x}{D}\right)^{1/3} \tag{2.1}$$

and u_1 is normalized by the inlet velocity, giving:

$$\frac{u_1}{U_\infty} = C_u \cdot \left(\frac{x}{D}\right)^{-2/3} \tag{2.2}$$

where C_b and C_u are proportional constants of b and u_1 respectively, x is the downstream distance behind the turbine, and D is the diameter of the wind turbine rotor. The constant C_b is calculated by plotting experimental values of normalized b against the normalized distance, both in a logarithmic scale, as is shown in figure 2.1. A linear line is created, which equation is calculated. Concurrently, the anaytical expression that defines the width for circular wakes, showed in table 2.1, is used for calculating b/D. Rewritten as $ln(b/D) = ln(C_b) + \frac{1}{3}ln(x/D)$, which has a similar distribution of a linear equation. Equating both intercept terms, the

line and the rearranged analytical expression, the parameter C_b can be determined. The proportional constant C_u for the velocity decay is calculated applying the same procedure.

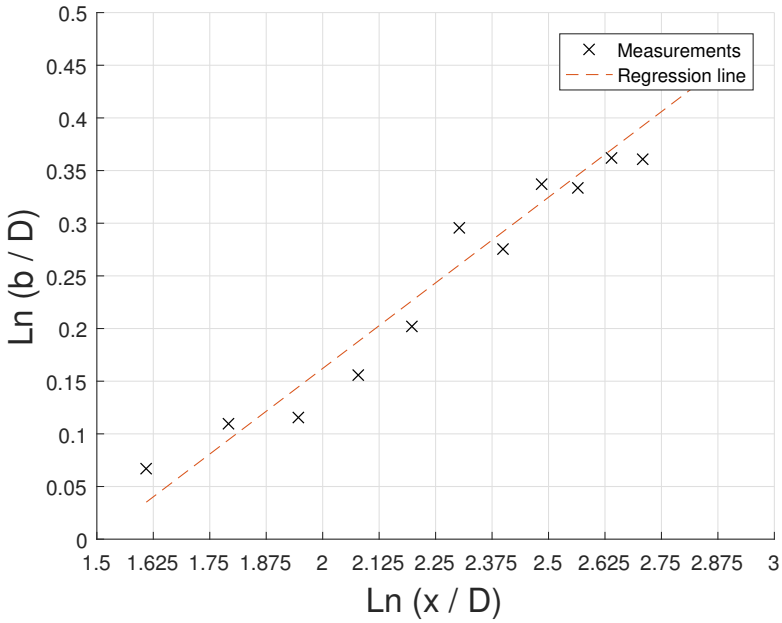

Figure 2.1: Plot of the experimental data for the calculation of the parameter C_b .

In table 2.2, the parameters used in the Schlichting model to compare it with the experimental data in two ambient turbulence intensity inflow conditions are shown.

	Low TI		High TI	
Parameter	C_b	C_u	C_b	C_u
Value	1.04	1.40	1.17	1.07

Table 2.2: The values for the parameters for the Schlichting model.

2.1.2 Jensen Model

Jensen model is one of the first analytical wake models [8]. It is derived from the momentum equation of the wind turbine. The wake behind the wind turbine is considered as a turbulent wake, which ignores the contribution of vortex shedding as they are only significant in the near wake region. Thus, this wake model is only valid in the far wake region. The velocity in the wake is given as a function of downstream distance from the turbine hub. It is assumed that the wake expands linearly downstream. To calculate the velocity decay, the wake velocity profile is considered constant inside the wake (known also as top hat profile, which can be seen in figure 2.2).

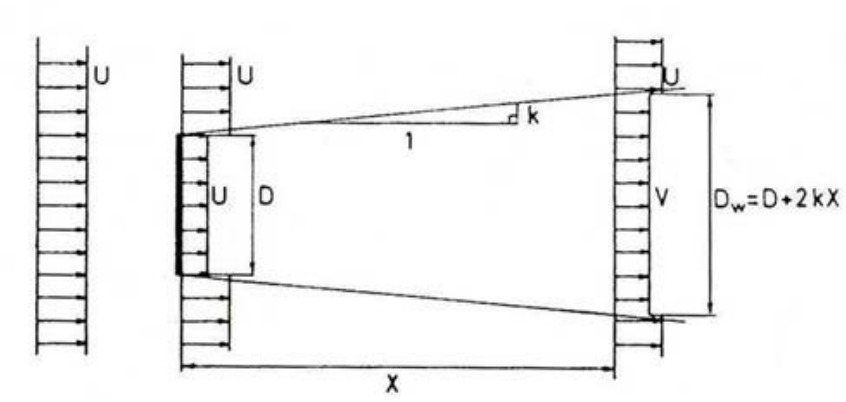

Figure 2.2: Sketch of the Jensen model [8], where the top-hat velocity profile can be identified

The expression to describe the width development is defined as:

$$D_{wake} = D \cdot (1 + 2 \cdot \kappa \cdot \frac{x}{D}) \tag{2.3}$$

And the expression for the velocity deficit u_{def} is defined as:

$$u_{def} = U_\infty \left[\frac{1 - \sqrt{1 - C_T}}{\left(1 + 2\kappa \frac{x}{D}\right)^2} \right] \tag{2.4}$$

where x is the downstream distance and D the diameter of the rotor. The decay factor κ describes how the wake expands by specifying the growth of the wake

width per unit downstream [8]. The determination of κ is a sensitive factors, where it is included the ambient turbulence, turbine induced turbulence and atmospheric stability. The recommended standard decay constants are 0.075 for onshore and 0.04-0.05 for offshore conditions. In [12] mentions that the factor k should fit to data at 4 D.

In table 2.3, the parameters used in the Jensen model to compare it with the experimental data under the two ambient turbulence intensity inflow conditions are shown.

	Low TI		High TI	
Parameter	κ	C_T	κ	C_T
Value	0.05	0.89	0.04	0.89

Table 2.3: The values for the parameters for the Jensen model.

2.1.3 Larsen Model

The derivation of the Larsen model is based on the Prandtl turbulent boundary layer equations [13]. The solutions to the wake width development and mean wake velocity decay can be obtained assuming a semi-similar velocity profile and using Prandtl's mixing length theory. Also, it is assumed that the wake flow is incompressible, stationary and axis-symmetric as the wind shear is neglected. The velocity decay is calculated by:

$$u_{def} = -\frac{U_\infty}{9}[C_T A(x+x_0)^{-2}]^{\frac{1}{3}}\left\{r^{\frac{3}{2}}[3\ {c_1}^2 C_T A(x+x_0)]^{-\frac{1}{2}} - \left(\frac{35}{2\pi}\right)^{\frac{3}{10}}(3c_1^2)^{-\frac{1}{5}}\right\}^2 \tag{2.5}$$

Where A is the area swept by the rotor, C_T is the thrust coefficient, U_∞ is the free-stream flow velocity and c_1 is a constant that shows the mixing length.

The wake width development can be expressed by:

$$D_{wake} = 2\left(\frac{35}{2\pi}\right)^{\frac{1}{5}}(3c_1^2)^{\frac{1}{5}}[C_T A(x+x_0)]^{\frac{1}{3}} \tag{2.6}$$

The constant c_1 is related to the mixing length and the constant x_0 represents the relative position of the turbine respect the coordinates system.

$$c_1 = \left(\frac{D_{eff}}{2}\right)^{\frac{5}{2}}\left(\frac{105}{2\pi}\right)^{-\frac{1}{2}}(C_T A x_0)^{-\frac{5}{6}} \tag{2.7}$$

$$x_0 = \frac{9.5D}{\left(\frac{2R_{9.5}}{D_{eff}}\right)^3 - 1} \tag{2.8}$$

Where D_{eff} is the effective rotor diameter expressed by:

$$D_{eff} = D\sqrt{\frac{1+\sqrt{1-C_T}}{2\sqrt{1-C_T}}} \tag{2.9}$$

The parameter $R_{9.5}$ is the wake radius at a relative distance of 9.5 rotor diameters downstream the wind turbine.

$$R_{9.5} = 0.5[R_{nb} + min(H, R_{nb})] \tag{2.10}$$

The ambient turbulence intensity is included in the parameter R_{nb}

$$R_{nb} = max(1.08D, 1.08D + 21.7D(I_a - 0.05)) \tag{2.11}$$

In table 2.4, the parameters used in the Larsen model to compare it with the experimental data in the two ambient turbulence intensity inflow conditions are shown.

	Low TI			High TI		
Parameter	I_a	C_T	$R_{9.5}$	I_a	C_T	$R_{9.5}$
Value	0.0023	0.89	1.20	0.105	0.89	1.22

Table 2.4: The values for the parameters for the Larsen model.

2.1.4 Frandsen Model

The Frandsen model [14] is based in a cylindrical control volume with constant cross-sectional is equal to the wake region. The shape of the flow speed can be shown by a constant distribution (top-hat velocity profile). An unique characteristic of this model is the consideration of the initial expansion of the wake. The

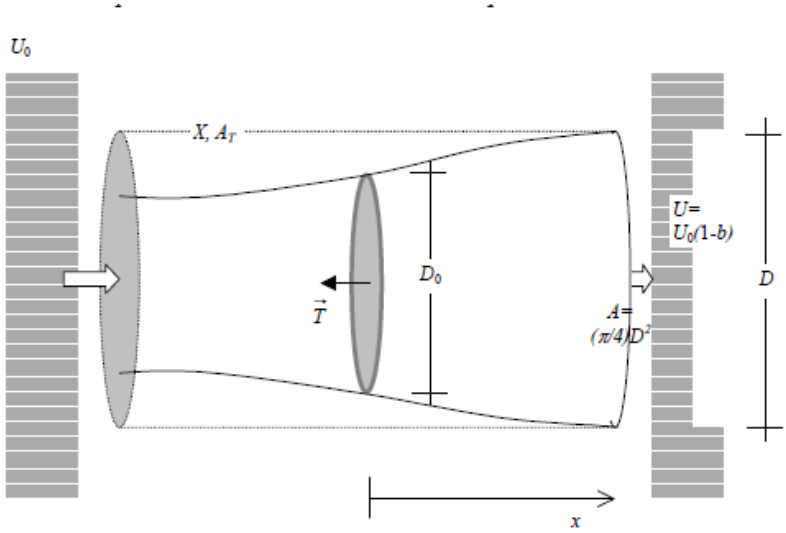

Figure 2.3: Diagram of the Frandsen's model. [14]

velocity decay is described as:

$$u_{def} = \frac{U_\infty}{2}\left(1 \pm \sqrt{1 - 2\frac{A}{A_{wake}}C_T}\right) \tag{2.12}$$

where A_{wake} is the wake impacting are corresponding to the wake width. For the $\pm$ sign, the (+) means the induction factor a ≤ 0.5 and the (-) when a > 0.5. The wake width development can be described as:

$$D_{wake} = D\left(\beta^{\kappa/2} + \alpha\frac{x}{D}\right)^{1/\kappa} \tag{2.13}$$

where β is the expansion parameter that its expression is:

$$\beta = \frac{1 + \sqrt{1 - C_T}}{2\sqrt{1 - C_T}} = \left(\frac{D_{eff}}{D}\right)^2 \tag{2.14}$$

the parameter α describes the initial wake expansion. The coefficients κ and α are found in the literature. In table 2.5, the parameters used in the Frandsen model to compare it with the experimental data in the two ambient turbulence intensity inflow conditions are shown.

	Low TI			High TI		
Parameter	α	C_T	κ	α	C_T	κ
Value	0.34	0.89	2	0.44	0.89	2

Table 2.5: The values for the parameters for the Frandsen model.

2.1.5 Ishibara Model

The Ishibara model [15] was developed by using wind tunnel data from a Mitsubishi wind turbine. An advantage compare with others models is that on this model take into account the turbulence intensity as input, which allows to adapt the model to different conditions. The velocity profile is assumed to be described as Gaussian shape. The velocity decay is described by:

$$u_{def} = \frac{\sqrt{C_T}U_\infty}{32}\left(\frac{1.666}{\kappa_1}\right)^2\left(\frac{x}{D}\right)^{(-p)} exp\left(-\frac{r^2}{D_{wake}^2}\right) \tag{2.15}$$

And the wake development can be calculated by:

$$D_{wake} = \frac{\kappa_1 C_T^{\frac{1}{4}}}{0.833} D^{1-\frac{p}{2}} x^{\frac{p}{2}} \tag{2.16}$$

where the parameter p is dependent on the turbulent intensity given by:

$$p = \kappa_2(I_a + I_w) \tag{2.17}$$

Where both terms, I_a and I_w represent the ambient turbulent and the turbine-generated turbulent respectively.

$$I_w = \frac{\kappa_3 C_T}{max(I_a, 0.03)}\left\{1 - exp\left[-4\left(\frac{x}{10D}\right)^2\right]\right\} \tag{2.18}$$

where the coefficients κ_1, κ_2 and κ_3 are found in the literature [15]. In table 2.6, the parameters used in the Ishibara model to compare it with the experimental data in the two turbulence intensity inflow conditions are shown.

	Low TI					High TI				
Parameter	I_a	C_T	κ_1	κ_2	κ_3	I_a	C_T	κ_1	κ_2	κ_3
Value	0.0023	0.89	0.27	5	0.004	0.105	0.89	0.27	6	0.004

Table 2.6: The values for the parameters for the Ishibara model.

2.2 Turbulence intensity

Three models are investigated in order to describe the downstream turbulence intensity development. It is important to predict the turbulence intensity to avoid fatigue loads produced by the velocity fluctuation in the wake of the upstream turbine. The analyzed models are based on correlations from wind tunnel experiments or measurement field campaigns. The turbulence intensity created by the wind turbine it is estimated and added to the ambient turbulence.

2.2.1 Crespo Model

Crespo and Hernandez [16] developed a model for the turbulence intensity created by the turbine. The expression was obtained by fitting with numerical results. The model is only valid for the far wake, as in the near wake an expansion occurs which is not considered in the model.

$$\Delta I \;=\; 0.73\, a^{0.83}\, I_{\infty}^{-0.0325} \left(\frac{D}{x}\right)^{0.32} \tag{2.19}$$

where the parameters a and I_∞ according to the theory should be between $0.1<a<0.4$ and $0.07<I_\infty<0.014$

In table 2.7, the parameters used in the Crespo model to compare it with the experimental data in the two turbulence intensity inflow conditions are shown.

	Low TI		High TI	
Parameter	a	I_∞	a	I_∞
Value	0.20	0.0023	0.18	0.105

Table 2.7: The values for the parameters for the Crespo model.

2.2.2 Quarton Model

A model was developed by Quarton [17] to describe the turbulence intensity development behind a wind turbine. The model is based on the Crespo model (subsection 2.2.1) which correlations are improved by fitting with experimental results, both wind tunnel and field experiments.

$$\Delta I = 4.8\, C_T^{0.6}\, I_\infty^{0.68} \left(\frac{\chi_N}{x}\right)^{0.57} \tag{2.20}$$

where C_T is the drag coefficient and χ_N is the near wake length, usually ranging between 1 D - 3 D

In table 2.8, the parameters used in the Quarton model to compare it with the experimental data in the two turbulence intensity inflow conditions are shown.

	Low TI			High TI		
Parameter	C_T	I_∞	χ_N	C_T	I_∞	χ_N
Value	0.89	0.0023	3	0.89	0.105	2.75

Table 2.8: The values for the parameters for the Quarton model.

2.2.3 Frandsen Model

Frandsen and Thogersen [18] during the study of the fatigue in wind turbines, developed a expression for the turbulence intensity based on measurements, where the constants are chosen to best fit with the data.

$$\Delta I = \frac{1}{1.5 \ + \ 0.3 \ (x/D) \ \sqrt{V_{hub}}} \tag{2.21}$$

where V_{hub} is related to C_T or to u which is the mean velocity at hub height. In table 2.9, the parameters used in the Frandsen model to compare it with the experimental data in the two turbulence intensity inflow conditions are shown.

	Low TI		High TI	
Parameter	V_{hub}	I_∞	V_{hub}	I_∞
Value	6.7	0.0023	9.4	0.105

Table 2.9: The values for the parameters for the Frandsen model.

Chapter 3

Experimental setup

In this section, the different instrumentation and the facilities used during the measurement campaigns are explained. A simple sketch of the experimental setup is presented in figure 3.1. Two main measurement campaigns were performed, one for the drag disk and another one for the turbine. In addition, for both of them, the ambient turbulent intensity was changed by including a grid at the inlet of the wind tunnel.

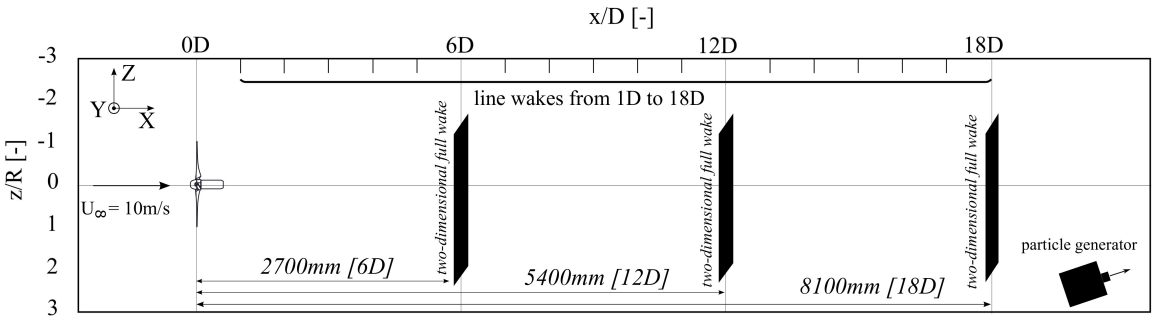

Figure 3.1: Sketch of the experimental set up in the wind tunnel.

3.1 Wind tunnel

The large close-loop wind tunnel at the Energy and Process Engineering Department place in Gløshaugen, NTNU was used in order to carried out the necessary experiments. The test area consist in a 1.80 x 2.72 m^2 cross section area (height x width) with a length of 12 m.

The inlet velocity (U_∞) was set to 10.0 m/s and kept constant during the wake measurements. That was verified by measuring the velocity of the incoming flow for every measurement point using the pressure difference at the contracted duct at the wind tunnel inlet. The procedure is explained further in detail in section 3.1.2. The turbine, which has a rotor diameter of 0.45 m, was installed at a distance 2.71 D downstream of the inlet of the wind tunnel. In order to correct the losses between the contraction and the place of the wind turbine a correction factor is used. The hub height was adjusted to 0.89 m to have the rotor in the center of the cross section of the wind tunnel.

Figure 3.2: Picture of the test section of the wind tunnel with the LDV probe mounted onto the traverse, wind turbine and the grid installed.

3.1.1 Turbulent grid

The inflow ambient turbulent intensity with empty inlet correspond to 0.23%. To test a second different inlet ambient turbulent intensity, a wooden grid is placed at the inlet of the test section, which is shown in figure 3.3. The grid is formed

by even distributed quadratic wooden spars of 47 *mm* side length leading in a mesh size of 240 *mm* space between them. Consequently, a uniform flow profile is created with a resulting inflow turbulent intensity of 10.5%.

Figure 3.3: Picture of the wind turbine with the grid installed at the inlet of the wind tunnel test section.

3.1.2 Contraction

To measure the inlet velocity, two static pressures were measure at the inlet contracted duct. Using Bernoulli equation (equation 3.1), and the area relation of the contraction (equation 3.2), assuming incompressible flow, the inlet velocity can be isolated (U_∞), as is shown in equation 3.3:

$$P_1 + \frac{1}{2}\rho U_1^2 = P_2 + \frac{1}{2}\rho U_2^2 \tag{3.1}$$

$$U_1 A_1 = U_2 A_2 \tag{3.2}$$

$$U_\infty = \sqrt{\frac{2\Delta p_{contraction}}{\rho\left(1 - \frac{A_2^2}{A_1^2}\right)}} \tag{3.3}$$

3.2 Traverse

In order to measure along the wind tunnel with accuracy, a mechanism called traverse was used. By installing the LDV probe in the arm of the traverse any position in the plane Z can be chosen. The traverse in controlled by a in-house LabView software. The movements are limited from - 2 D to 2 D in the $Y - axis$ and from - 2 D to 2 D in the $Z - axis$. The movements in the $X - axis$ are done manually by moving the traverse to the desired position. The movement is possible between 0 D and 15 D downstream the wind turbine. Up to 18 D is possible to reach, however, the traverse has to be moved underneath the frame that hold the traverse and, as is shown in section 4, that creates interference with the wake expansion. As a result, the study in the $X - axis$ will be limited to 15 D.

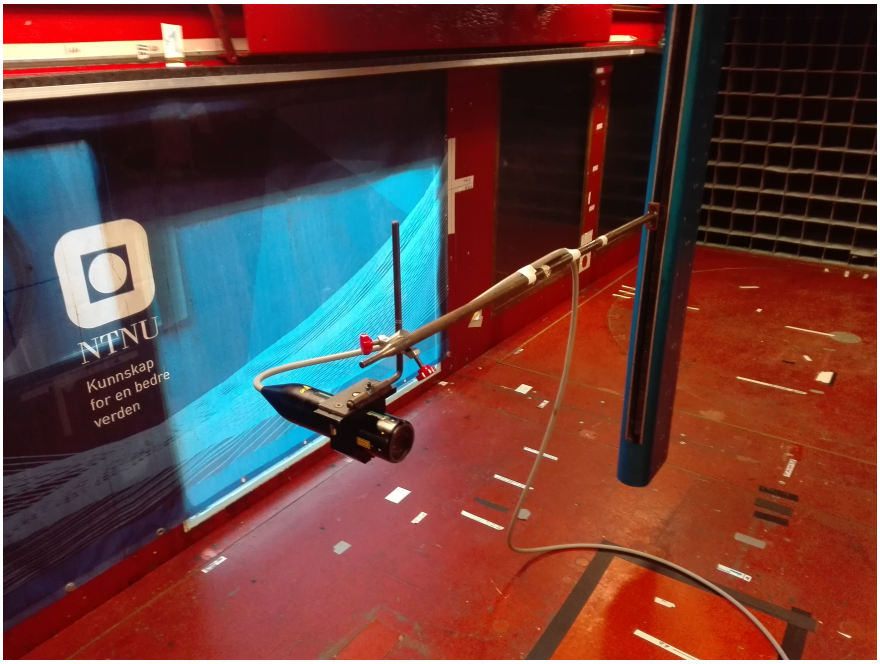

Figure 3.4: Picture of the traverse with the LDV probe installed.

3.3 Drag disk

Figure 3.5: Picture of the drag disk installed in the wind tunnel.

It is needed to check if the model derived by Schlichting can be applied to a wind turbine. To validate it, a comparison of the behavior of the far wake between a blunt body and a wind turbine is performed. A drag disk is manufactured, and different C_T values can be chosen by moving one plate over the other. At different positions the C_T are measured in the balance installed in the wind tunnel. The C_T values are shown in the table 3.1

	Low TI					High TI				
Parameter	Pos 1	Pos 2	Pos 3	Pos 4	Pos 5	Pos 1	Pos 2	Pos 3	Pos 4	Pos 5
Value	0.96	0.99	1.12	1.22	1.26	1.06	1.12	1.25	1.37	1.45

Table 3.1: The values for the C_T for different drag disk positions.

3.4 Turbine

A new turbine is used in the measurement campaign. The new rotor is based on the rotor developed at the Department of Energy Process Engineering at NTNU Trondheim which is described in detail by Krogstad and Lund [19]. The new

Figure 3.6: Picture of the wind turbine installed in the wind tunnel.

rotor is also based on the NREL S826 airfoil, however the blade parameters are modified to get a smaller rotor diameter. Blade parameters such as twist and the chord distribution were not changed. As a result, the new rotor has a diameter of $0.45m$. Also the nacelle and the tower are smaller compared with the reference rotor, which as a result smaller interference to the wake is expected. Parameters such as drag and thrust coefficients are calculated.

This smaller rotor was designed to be able to investigate the far wake and thus, a larger range behind the turbine. Blockage effects and wake interference with the wind tunnel walls should be as small as possible such that the wake can develop without being contracted [3]. Compared with the reference rotor, which has a wind

tunnel blockage ratio of around 13%, the new rotor has only a blockage ratio of around 3%. In order to avoid the interference between the measurements and the walls of the wind tunnel a limit of 10% blockage ratio is recommended [20]. Hence, it is expected that the wake can expand without being influence by the wind tunnel walls. The single rotor blades were produced with a 3D printer based on the multi-jet technology and connected at the hub with metal rings. The assembly of the rotor in the wind tunnel is shown in figure 3.6. With this assembly, the power coefficient (C_P) and thrust coefficient (C_T) for the new rotor were measured, which results are presented in figure 3.7. The optimum tip speed ratio (TSR) for the new rotor is 3.5 and is marked in figures 3.7a and 3.7b by a red cross. All the wake measurements were conducted at the optimum TSR of 3.5.

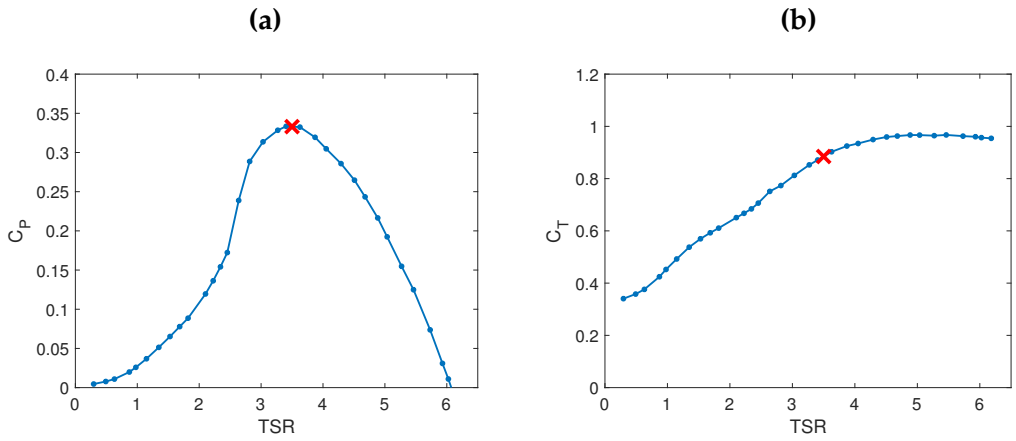

Figure 3.7: Experimental results for (a) C_p and (b) C_T over TSR. The red X marks the TSR where all the wake measurements were conducted.

3.5 Laser Doppler Velocimeter

A two-component Laser Doppler Velocimetry (LDV) probe was used to measure the velocity components. It was mounted onto a traverse in order to move the LDV probe in the wind tunnel. The main principle of the LDV is the fringe model. The fringe model is based on the visualization of the two intersecting beams form

a fringe pattern of high and low intensity. When the particle traverses this fringe pattern, the scattered light fluctuates in intensity with a frequency equal to the velocity of the particle divided by the fringe spacing [21].

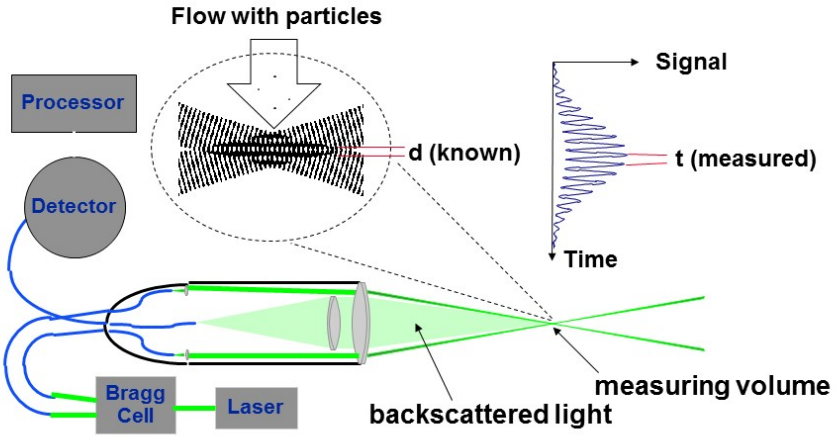

Figure 3.8: Operation diagram of a Laser Doppler Velocimeter [21]

The LDV provides several advantages compared with other techniques as pitot probe. LDV is a non intrusive measurement technique, does not need calibration as it is an absolute measurement technique. In order for the LDV probe to detect the airflow, a small smoke machine generating particles with a size of 0.5-2.0 μm was placed at the back of the wind tunnel. As the wind tunnel is closed-loop type, the particles were evenly distributed in the airflow during the returning process. 50 000 samples measured with the LDV probe were collected at every measuring point. This high number is due to the variations in the wake and reduce the uncertainty caused by the turbine. In that way is reached a final uncertainty of 7.3% in the measurements.

Chapter 4

Results

Two different sets of experiments were carried out. For both types, two different ambient turbulence intensity condition were performed by installing the grid at the inlet. In the first set, three full wakes in the zy-plane were measured at distances in the x-direction of 6 D, 12 D and 18 D behind the turbine. The measured area for the full wakes was ranging from -1.33 D to 1.33 D in z-direction, and from -1.07 D to 1.07 D in y-direction, with the center located at the rotor axis. With an increment of 0.13 D (0.06 m) in both directions, resulting in a measurement grid of 357 points.

The second set consist in 1 D line wake measurements in z-axis. Lines were performed at every downstream distance D from the turbine, ranging from 1 D to 15 D. The z-axis remained the same, ranging from -1.33 D to 1.33 D, as well as the increment size, 0.10 D. In the experiments were the grid was not installed a lower y-value than the rotor axis was chosen, at a center line 0.22 D (0.10 m). This value was chosen due to the center of the wake shifted downward behind the turbine, which was observed from the full wake measurements which are presented in detail in the section 4.2. In the cases were the grid was installed this downshift in the y-axis was not needed, also explained further in detail in chapter 4.2.

4.1 Drag Disk

A experiment was performed to measure the wake behind a drag disk. The position between the two plates of the drag disk give a resultant C_T equivalent to the

C_T of the wind turbine at 3.5 TSR, which can be seen in table 3.1. The contour plots of the measured lines in the z-axis from 1 - 15 D are shown in figure 4.1. The result from the velocity measurement under low ambient turbulence conditions is shown in figure 4.1b and the result for high ambient turbulence condition is shown in figure: 4.1a.

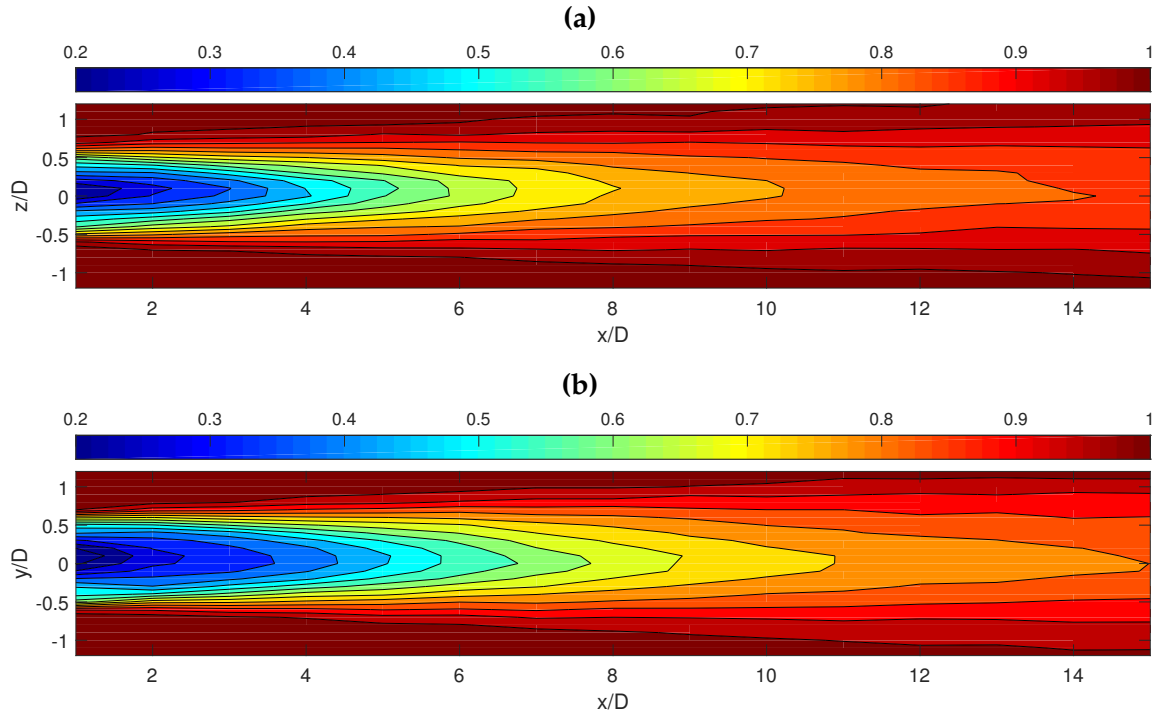

Figure 4.1: Velocity full wake plots of the drag disk from a distances of 1 D to 15 D for (a) high ambient turbulence condition and (b) low ambient turbulence condition behind the wind turbine.

As expected, the wake shows a recovery of the velocity decay as it is moving downstream the turbine. Also, an axis-symmetric behaviour for all the wake is observed, thus the near wake is considered to be shorter than 1 D. In the case were the grid was installed, as the ambient turbulent intensity is higher, the mixing between the wake and the surrounding flow is higher, which as a result, the required recovery distance is lower and the velocity decay recovers faster. Similar behaviour is commented in [3] and [9].

4.2 Velocity decay

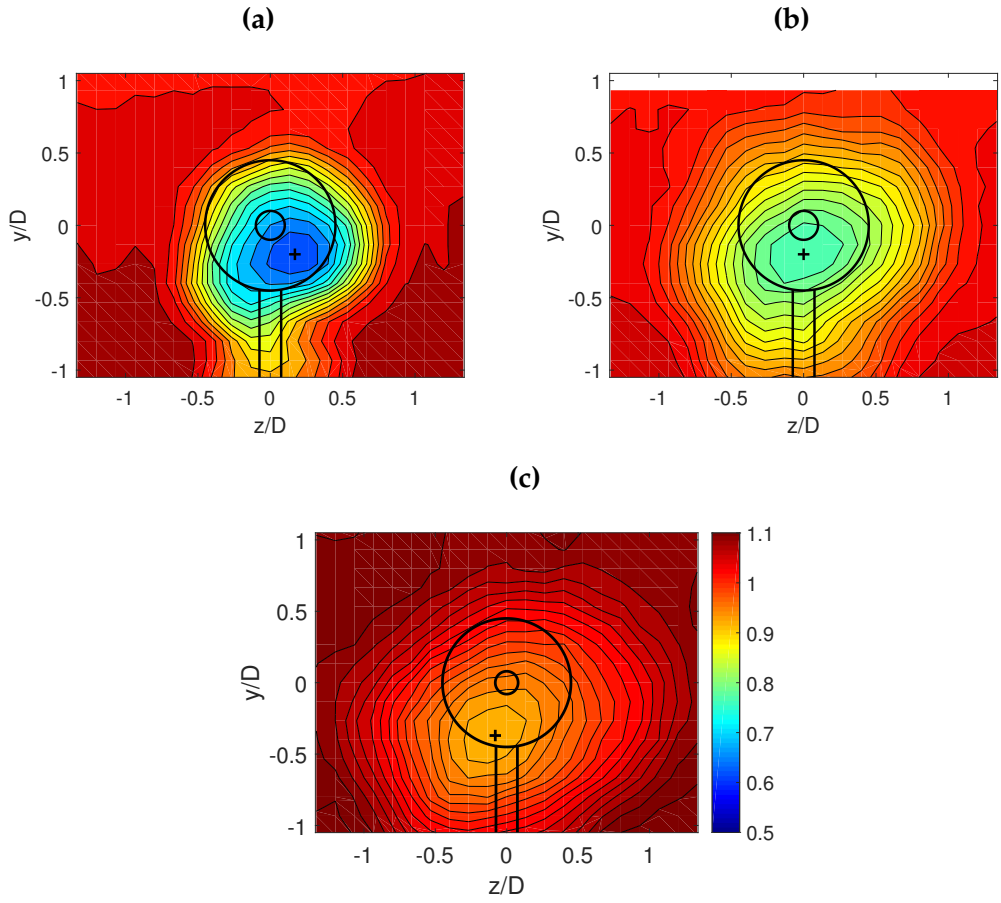

Figure 4.2: Two-dimensional velocity full wake plots in zy-plane for low ambient turbulence intensity at distances of (a) 6D, (b) 12D, and (c) 18D behind the turbine with a rotor diameter of 0.450 m. The plus sign (+) in the plots marks the center of the wake.

In figures 4.2a, 4.2b and 4.2c, two-dimensional contour plots of the full wake for low ambient intensity turbulence in the zy-plane are presented at distances of 6 D, 12 D and 18 D, respectively. The velocity decay decreases as the wake moves downstream. The development of the wake can be seen, with an expansion of the wake as the downstream distance increases. This behaviour was expected as previous work has already shown the same wake development [9]. In all three cases, a downshift of the center line of the wake can be observed. This is assumed to be

due to interactions of the wake and the turbine tower, the effect was investigated in detail by Pierella [22]. Consequently, the line measurements were measured at a distance 0.22 D below the rotor axis as this is where the wake center was located, its position is marked in figure 4.2 by a plus sign (+).

At 6 D and 12 D, the wake is approximately circular, whereas at 18 D a larger expansion in horizontal direction can be observed. This is expected to be due to interference with the traverse in the back of the wind tunnel since, from 16 D - 18 D, the LDV probe had to be placed beneath the framework supporting the traverse. This resulted in a contraction of the cross section and thus, a compression of the flow in y-direction. Consequently, the measurements from 16 D to 18 D are not considered in the evaluation of the analytical models.

For the experiments with higher ambient turbulence, the center of the wake remains at hub height, as can be appreciated in figure 4.3, where the velocity was measured in a small grid of 0.1 D step ranging $\pm$0.25 D in vertical and horizontal directions at hub height, 15 D downstream the wind turbine. Thus, the line measurements for the high ambient turbulence conditions were performed at hub height. Same interference is expected between the wake and the framework of the traverse, as with higher mixing the wake expands more. Thus, also for the high ambient turbulence the distance is limited to 15 D.

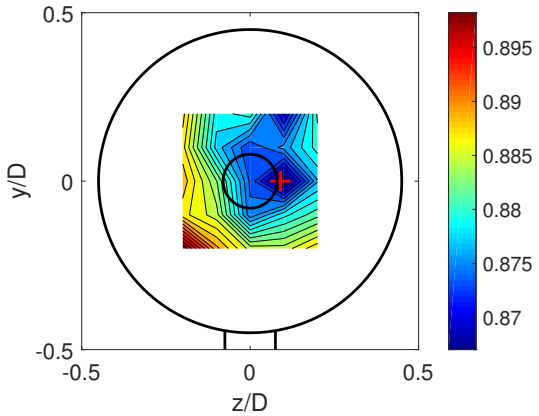

Figure 4.3: Two-dimenstional velocity wake under high turbulence conditions, centered on the rotor axis 15 D downstream the turbine. The red plus sign (+) in the plot marks the center of the wake

4.3 Width development

In order to analyzed how the wake was developing with increasing distance downstream from the turbine, a counter plot of the velocity development of the lines from 1 D to 15 D is shown in figure 4.4a.

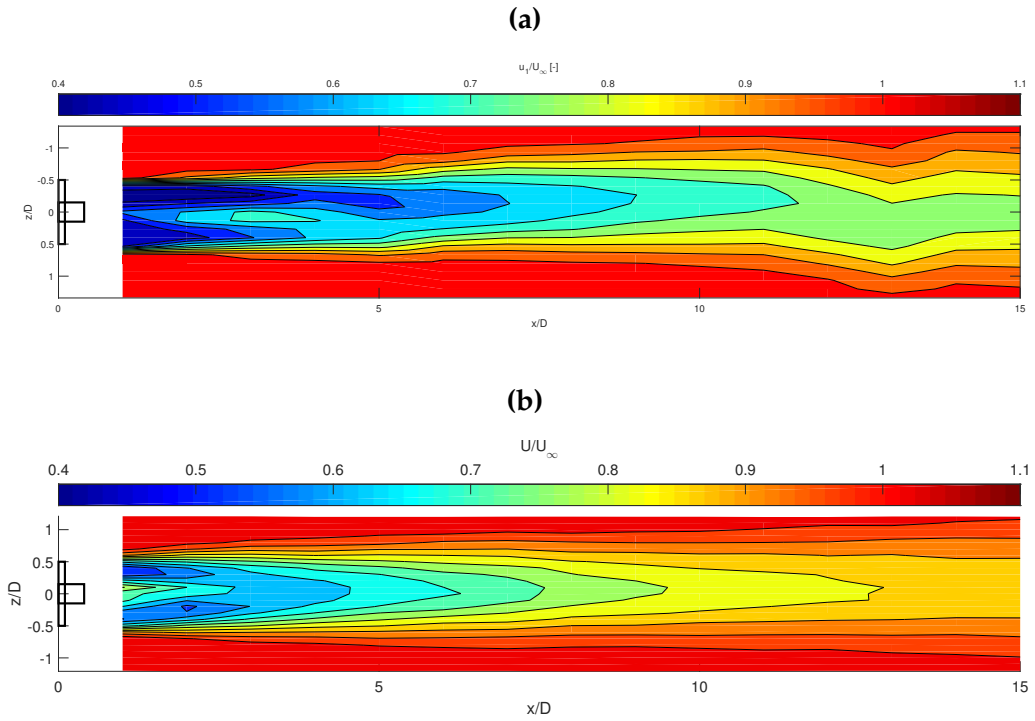

Figure 4.4: Velocity profiles of the wake in the xz-plane with a center line at y = -0.22 D.

The highest velocity deficit is found in the near wake region, whereas, as expected, the velocity increase as it moves downstream the turbine due to turbulent mixing. In the near wake the influence of the turbine geometry is still dominant and can clearly be observed by the two peaks in the velocity deficit. Thus, the velocity distribution in the near wake is not symmetric. However, with increasing distance the wake is getting more symmetric and is considered to be fairly axisymmetric in the far wake.

Similar behaviors are appreciated between the two different ambient turbulence

intensities. As expected, with higher turbulence intensity, the width of the wake is wider and the velocity decay is smaller compared with a lower ambient turbulence intensity. The near wake is also smaller in the high ambient turbulence intensity case.

4.4 Turbulent Intensity

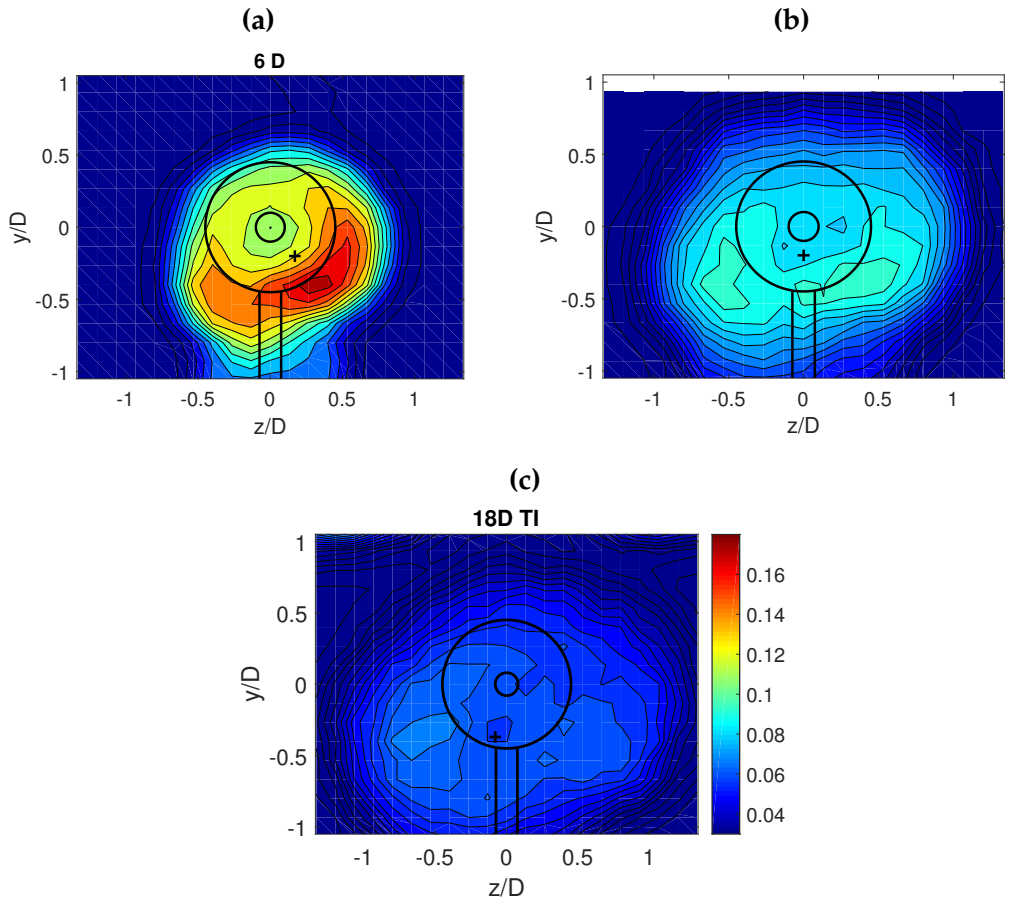

Figure 4.5: Two-dimensional turbulence intensity wake plots at distances of (a) 6D, (b) 12D, and (c) 18D behind the turbine with a rotor diameter of 0.450 m.

In figures 4.5a, 4.5b and 4.5c, two-dimensional contour plots of the turbulence intensity full wake are presented at distances of 6 D, 12 D and 18 D. It is observed

that the turbulence intensity in the wake of the turbine is increased with respect to the inflow turbulence intensity. This is expected, as the turbine adds turbulence to the ambient conditions. Also, as expected, the turbulence intensity decreases as the wakes moves downstream. The decrease is slower compared with the recovery of the velocity deficit, also mention in [3].

As was explained in section 4.2, the measurements from the wake at distances 16 D to 18 D are discarded. It can be seen in figure 4.5c the influence of the traverse with an increase of the turbulence intensity on the top of the full wake.

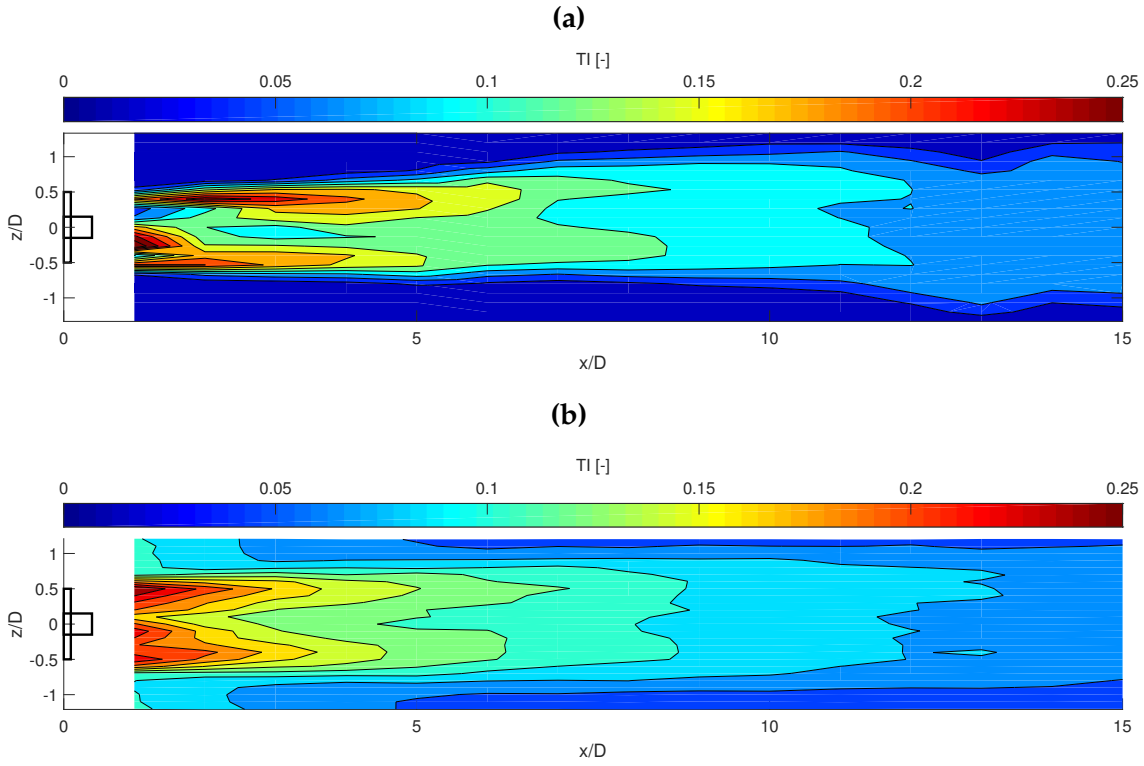

Figure 4.6: Two-dimensional turbulence intensity full wake plots in zy-plane at distances of (a) wind turbine without grid and (b) wind turbine with grid behind the turbine.

In figure 4.6, both cases show a symmetric behavior in the far wake. Also, a two peak structure is observed in the near wake, which corresponded to the tip vortices [23]. In 4.6b, where the ambient turbulence intensity is higher, due to turbulent mixing, those two peak structure moved less further downstream the

turbine compared with the low ambient turbulence intensity. Also, the recovery of the turbulence intensity in the wake is faster when the ambient turbulence intensity is higher.

Chapter 5

Discussion

In this chapter the results of the experiments are discussed.

5.1 Study of the wake behind a drag disk

It is study the viability of the Schlicting model by analyzing if the wake of a wind turbine behave as the wake of a blunt body. The results from the experiment can be seen in figure 5.1. On them, in the near wake, the velocity decay of the drag disk shows a stepper linear behavior compared with the wind turbine. In the far wake region, from 6 D, both the drag disk and the wind turbine a convergence behavior can be appreciated.

Analyzing the width development, figure 5.2, in the analyzed range, 1 D to 15 D, the wake of the drag disk and the wind turbine shows a similar behavior. However, there is an small offset between them. The ambient turbulence does not show any different impact between the wake of the drag disk and the wind turbine, as for both, same effect can be appreciated.

Thus, Schlichting model which was derived for blunt bodies, can be applied to describe the far wake of a wind turbine as the wake of both of them are similar or proportional.

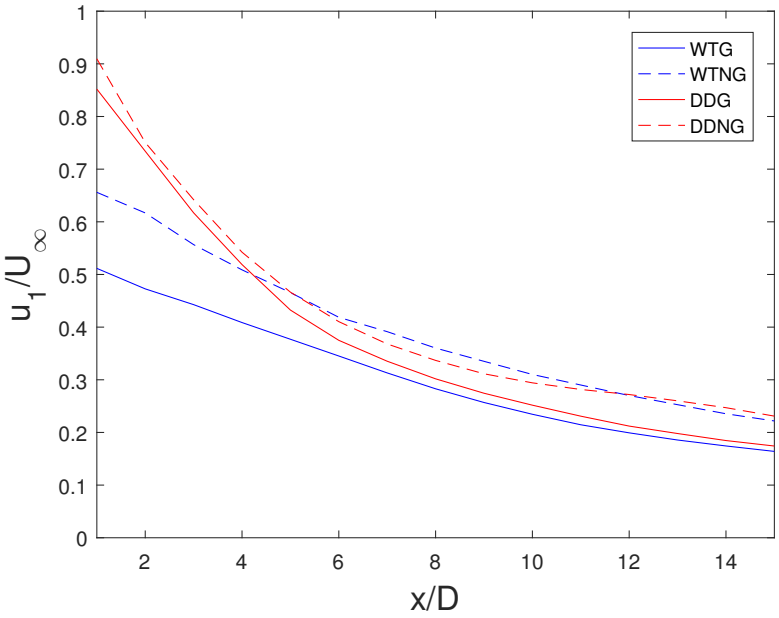

Figure 5.1: Comparison of the velocity decay of the wake between a drag disk (DD) and a wind turbine (WT) in two ambient turbulence intensity cases. Low ambient turbulence intensity (NG) and high turbulent intensity (G) from 1 D to 15 D downstream

5.2 Influence of the ambient Turbulence Intensity

In figures 5.1 and 5.2, a comparison of the effect of the ambient turbulence intensity of the flow in a wind turbine (blue full/dash lines) can be observed. It is appreciated that it is a parameter to be considered as it affects both wakes characteristics, velocity decay and width development. For the velocity decay, with higher ambient turbulence intensity the initial velocity decay is approximately 66.4%, whereas a lower value of 51.3% is obtained when the same experiment is performed with lower turbulent intensity. Also, the recovery distance of the velocity decay is lower, around a 24.8%. Those effects were expected as the mixing in higher ambient turbulence is higher as was reported in [3].

Analyzing the width development, with lower turbulence intensity it is needed more distance downstream to do not see the effects of the wake on the flow compared with higher turbulence intensity. The expansion of the wake is higher,

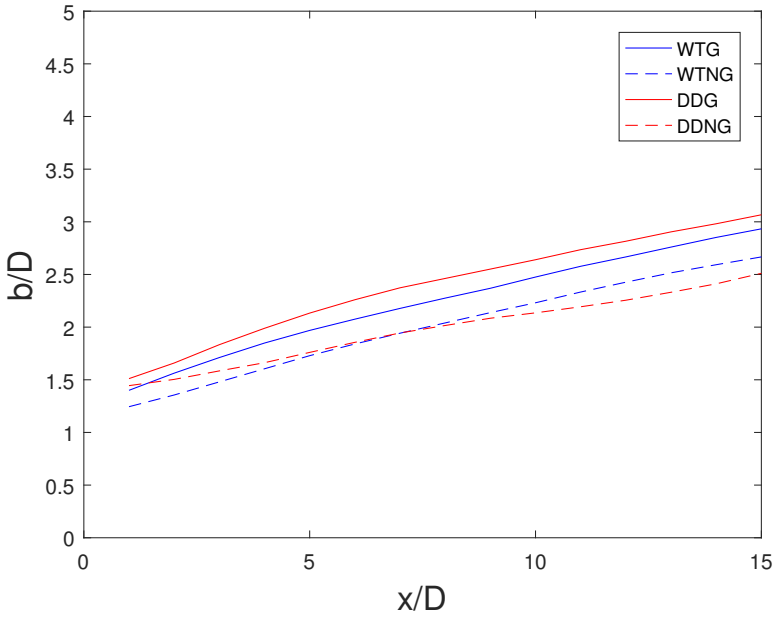

Figure 5.2: Comparison of the width development of the wake between a drag disk (DD) and a wind turbine (WT) in two ambient turbulence intensity cases. Low ambient turbulence intensity (NG) and high turbulent intensity (G) from 1 D to 15 D downstream

around a 18.6%, with higher turbulence intensity as it mix faster with the surrounding flow [23].

5.3 Velocity decay

Mean velocity decay is compared for the five models with experimental data for two different ambient turbulent intensities. In figure 5.3 the comparison between the models and the velocity decay in low ambient turbulence intensity conditions is shown. It can be clearly seen that most of the models cannot predict the near wake, $<$ 6 D, only Larsen model can predict roughly with an error of around 8%. As can be seen in figure 4.4a, the near wake extend longer than expected around 2 D - 5 D downstream the wind turbine as is suggested by Crespo et al [10]. However, the low turbulence intensity lead in a low mixing of the wake and as a result it is needed longer distance for the wake to fully develop. Also Helmis et all

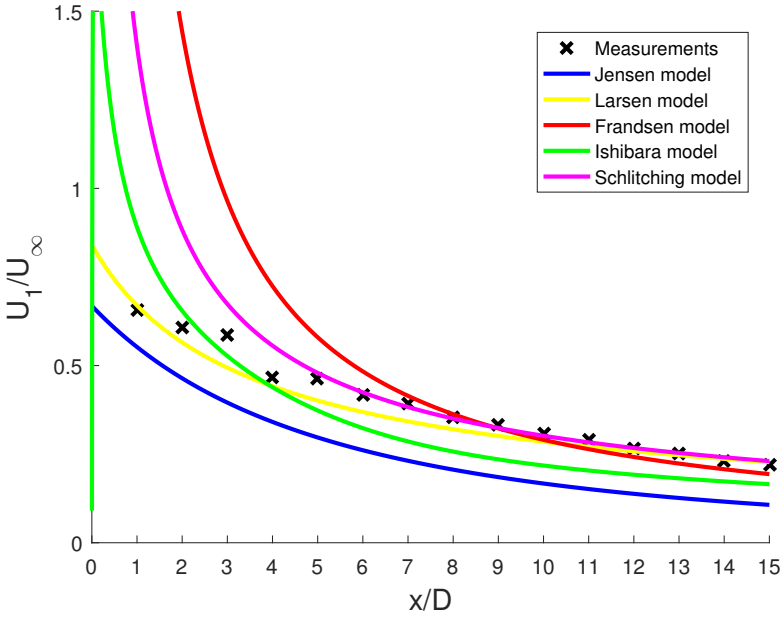

Figure 5.3: Comparison of the velocity decay of the experimental result with the studied models, under low ambient turbulence intensity conditions from 1 D to 15 D behind the turbine

[24] reported that near wake region is overestimated in wind tunnel experiments as the velocity deficit is higher in wind tunnel data.

In the far wake, $>$ 6 D, Jensen model and Ishibara model show a deviation of 44.8% and 26.5% respectively. The reason to this error might be the low ambient turbulence intensity of 0.23% which is a non realistic value. Jensen model might due to its simplicity might not consider that extreme low value, and Ishibara as was based on wind turbine correlations, might not considered an unrealistic value. For Larsen, Frandsen and Schlichting model accuracy increase considerably with a deviation of 6.7%, 8.6% and 2.0% respectively. The deviations from each model are summarize in the table 5.1:

Models	Jensen	Larsen	Frandsen	Ishibara	Schlichting
Error [%]	45.76	6.69	8.66	27.16	2.03

Table 5.1: The values of the deviation of the velocity decay in the far wake of the analyzed models under low ambient turbulence intensity.

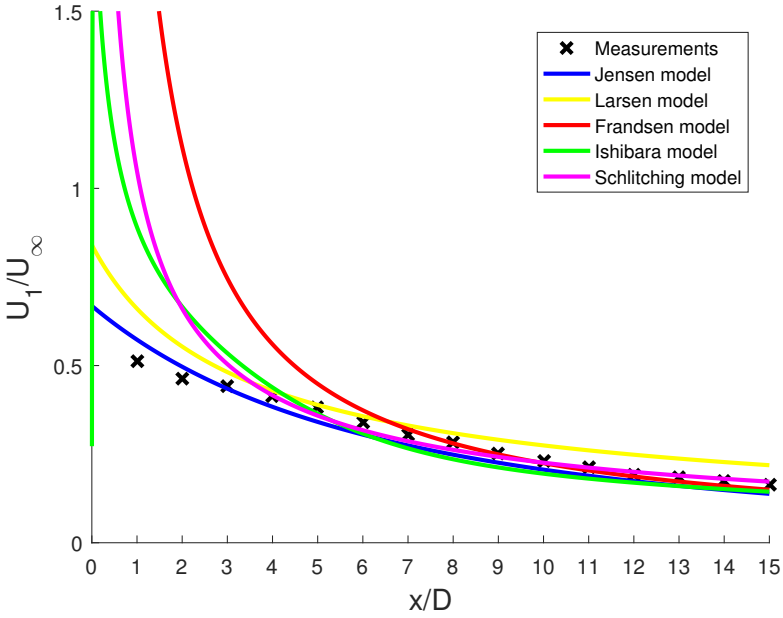

Figure 5.4: Comparison of the velocity decay of the experimental result with the studied models. and high turbulent intensity (b) from 1 D to 15 D behind the turbine

For higher ambient turbulence intensity conditions, shown in figure 5.4, the models seems to behave better compared with the results of low ambient turbulence intensity. Same observation is appreciated regarding the near wake, which none of the models can predict accurately the behaviour of the wake, which is expected due to the assumptions of the models. However, as the ambient turbulence intensity is higher, the near wake is shorter, reaching < 4 D, which belongs to the expected range as Crespo [10] suggested. The average deviation of the models is lower, around a 10%, with the Schlichting model as the best performance, just an average deviation of 4.3%. Larsen model shows a similar behaviour as the experimental data, however, an offset can be appreciated. The deviations from each model are summarize in the table 5.2:

Models	Jensen	Larsen	Frandsen	Ishibara	Schlichting
Error [%]	11.79	18.31	6.07	12.89	4.30

Table 5.2: The values of the deviation of the velocity decay in the far wake of the analyzed models under high ambient turbulence intensity conditions.

5.4 Width development

Experimental results of the width development downstream the wind turbine are compared with the five models for two ambient turbulence intensities. Figures 5.5 and 5.6 show the results for the low turbulence case and the high turbulence case respectively. Similar behavior as for the velocity decay explained in section 5.3 is observed. With a low ambient turbulence intensity, the deviation between

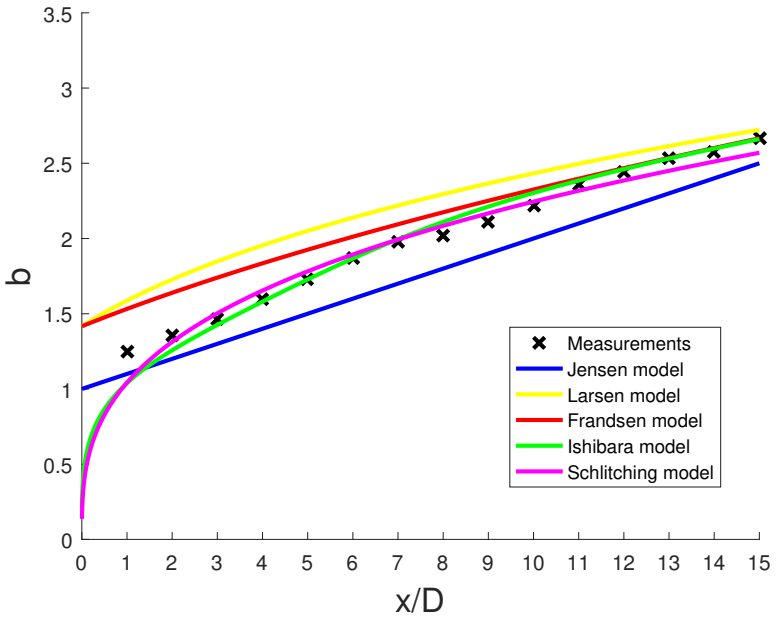

Figure 5.5: Comparison of the width evolution evolution of the wake between the different models with the turbulence intensity case II.

the models and the experimental results are divided into two groups. Jensen and Larsen deviates around 10%, whereas Frandsen, Ishibara and Schlichting show an

average deviation of 2.5%. Those deviations are calculated considering only in far wake, $>$ 6 D. The deviations from each model are summarize in the table 5.3

Models	Jensen	Larsen	Frandsen	Ishibara	Schlichting
Error [%]	10.54	9.05	4.30	1.54	2.29

Table 5.3: The values of the deviations of the width development under low ambient turbulence intensity conditions of the analyzed models.

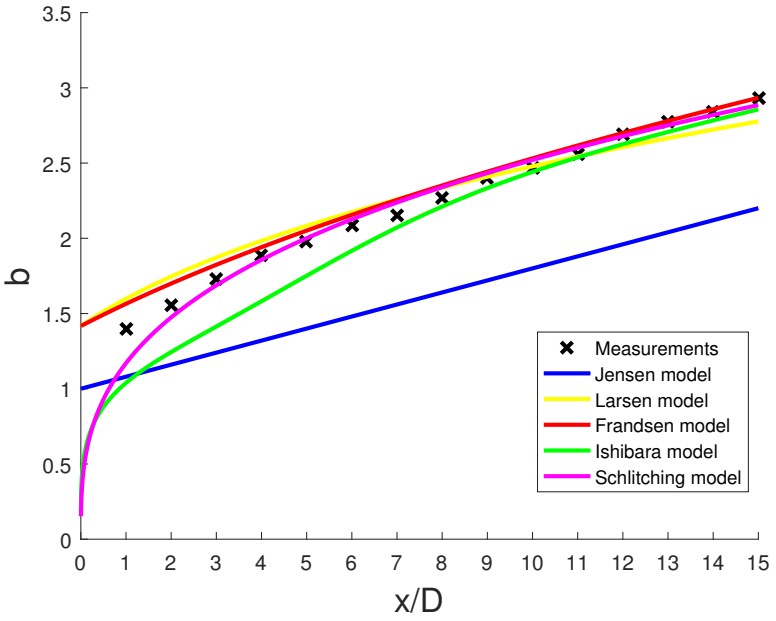

Figure 5.6: Comparison of the width evolution evolution of the wake between the different models under high turbulence intensity conditions.

In the case of high ambient turbulence intensity, the models behave much more accurately, with an average deviation of 2%, without including the Jensen model which as was observed for the velocity decay the deviation is around 27%. In the Jensen model the deviation is around constant when moving downstream, meaning that the initial expansion of the wake is not modelled properly. The deviations from each model are summarize in the table 5.4

Models	Jensen	Larsen	Frandsen	Ishibara	Schlichting
Error [%]	27.23	3.20	2.09	3.65	1.75

Table 5.4: The values of the deviations of the width development under high ambient turbulence intensity of the analyzed models.

5.5 Turbulence Intensity

Three analytical models for turbulence intensity of the wake (Crespo, Quarton and Frandsen) are compared with experimental data with two different ambient turbulence intensity. In figure 5.7 the results for a ambient turbulence intensity of 0.23% are shown and in figure 5.8 the results for a ambient turbulence intensity of 10.5% are shown. The case of high ambient turbulence intensity can be compared to an offshore situation. In the first case, under the low turbulence intensity condition is represented in figure 5.7. Frandsen model shows the best degree of agreement with only a 3.73% of deviation in average, whereas, Crespo model has a 14.62%. Quarton model deviates 74.63% which is not acceptable. The ambient turbulence intensity is very low, 0.23%, which only is possible in wind tunnels and might not be expected. The deviations from each model are summarize in the table 5.5

Models	Crespo	Quarton	Frandsen
Error [%]	14.62	74.63	3.73

Table 5.5: The values of the deviations of the turbulence intensity development under low ambient turbulence conditions of the analyzed models.

In figure 5.8 the comparison between the prediction of the models and the measurements under high ambient turbulence condition is shown. The measurement point is chosen at the maximum turbulence intensity for each measured distance.

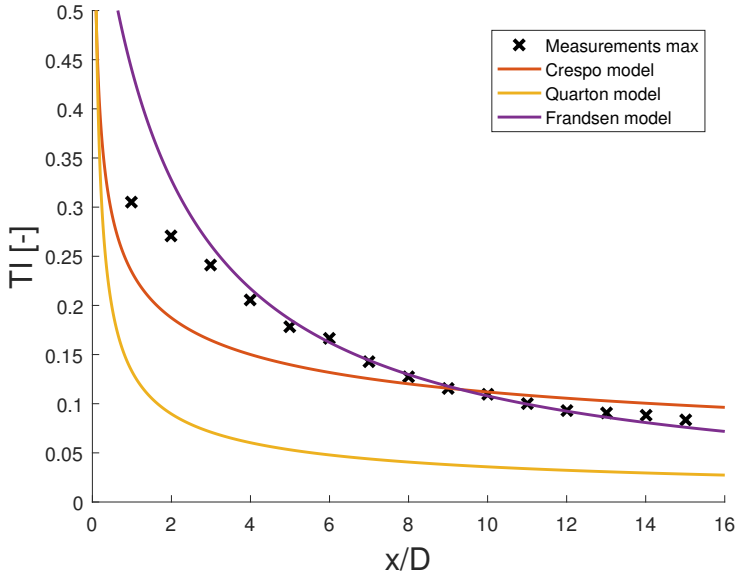

Figure 5.7: Comparison of the turbulence intensity of the experimental result with the studied models.Low ambient turbulence intensity (a) and high turbulent intensity (b) from 1 D to 15 D behind the turbine

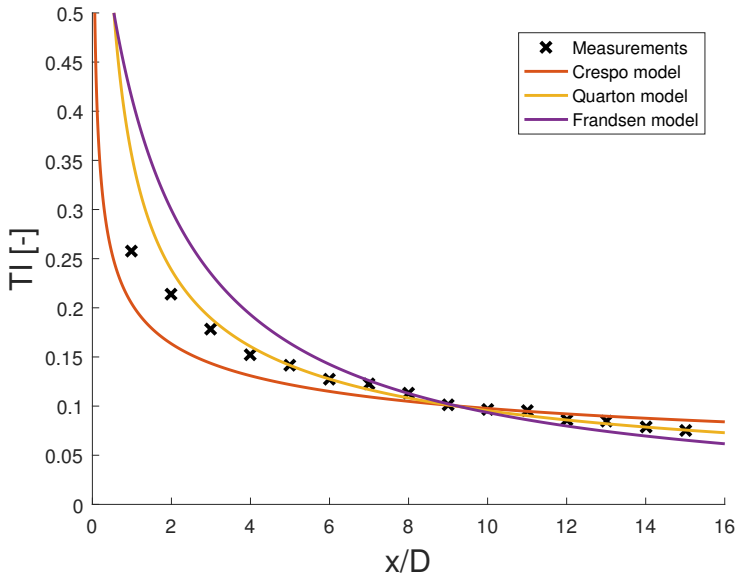

Figure 5.8: Comparison of the turbulence intensity of the experimental result with the studied models.Low ambient turbulence intensity (a) and high turbulent intensity (b) from 1 D to 15 D behind the turbine

Similar trend is observed in the three models. The Quarton model is the most accurate with an average deviation of 2.65%, follow by Crespo and Frandsen with 9.01% and 11.32% respectively. It is expected that the Quarton model performs better that Crespo as it is an improvement version.

The deviations from each model are summarize in the table 5.6

Models	Crespo	Quarton	Frandsen
Error [%]	9.01	2.65	11.32

Table 5.6: The values of the deviations of the turbulence intensity development under high ambient turbulence conditions of the analyzed models.

Chapter 6

Conclusion

Several analytical wake models were investigated in order to be applied on the prediction of wind turbine wakes characteristics. Results of the five analytical expressions for the velocity decay and the width development were compared to experimental results of the wake formed behind a model wind turbine for two cases of turbulence intensity. Also, three models for the added turbulence intensity were compared.

An studied was performed in order to check the viability of using a wake model for blunt bodies to the wake of a wind turbine. The study shows that the wake behind a drag disk is comparable to the wake behind a wind turbine.

It is observed that the ambient turbulence intensity is a main factor which affects the wake characteristics, with an increase of the width of 18% and a fast recovery of the velocity decay by 15% when an ambient turbulence intensity of 0.23% is compared with an ambient turbulence intensity of 10.5%.

For a low ambient turbulence condition, which only can be obtained in wind tunnel experiments, the analyzed models show a larger average deviation compared with a higher ambient turbulence condition case. This can be explained as some of the models are correlations based on measurements from field, which such a low ambient turbulence intensity is not included.

To describe both, the velocity decay and width development Schlichting is the model which present a more accurately prediction with an average deviation of 2.5% in all different ambient turbulence intensity condition. However, good degree of agreement is expected, as experimental data is included to calibrate the

parameters.

The three studied models for the turbulence intensity show that also behaves depending on the ambient turbulence intensity. A scattered results from the turbulence intensity models are obtained with a deviation between 3% and 10%. The near wake is not described well for none of the models. With high ambient turbulence conditions, Quarton model is the most accurate model with an average deviation of 2.65%.

Consequently, it can be concluded that analytical models for velocity decay and width development are able to predict the wake characteristics of a wind turbine rotor. Also, the turbulence intensity models perform fairly well.

Chapter 7

Further research

This project can be used as starting point for several research lines:

1. Validation of the analytical methods in field experiments
    - Study the impact of parameters in model and the performance.
    - Evaluation of models with atmospheric boundary layer inflow conditions.
2. Study the deflection of the wake under yaw conditions.
    - Use the deflection to decrease the interference between wind turbines.

Bibliography

[1] R. H. Wiser and M. Bolinger, "2015 wind technologies market report", 2015.

[2] E. P. C. of the European Union, "Directive 2009/28/ec of the european parliament and of the council of 23 april 2009 on the promotion of the use of energy from renewable sources and amending and subsequently repealing directives 2001/77/ec and 2003/30/ec", 2009.

[3] L. Vermeer, J. Sørensen, and A. Crespo, "Wind turbine wake aerodynamics", *Progress in Aerospace Sciences*, vol. 39th, pp. 467–510, 2003.

[4] D. Medici and P. Alfredsson, "Measurements on a wind turbine wake: 3d effects and bluff body vortex shedding", *Wind Energy*, vol. 9th, pp. 219–236, 2009.

[5] J. Sørensen and V. Okulov, "Modeling of the far wake behind a wind turbine",

[6] D. Renkema, "Validation of wind turbine wake models", Master's thesis, Delft University of Technology, 2007.

[7] H. Schlichting, *Boundary-layer theory*, 7. ed. McGraw-Hill, 1979.

[8] N. O. Jensen, I. Katic, and J. Højstrup, "A simple model for cluster efficiency", European Wind Energy Association, 1986.

[9] B. Sanderse, "Aerodynamics of wind turbine wakes: Literature review", *ECN*, vol. ECN-E-09e016, 2009.

[10] A. Crespo, J. Hernandez, and S. Frandsen, "Survey of modelling methods for wind turbine wakes and wind farms", *Wind Energy*, vol. 2nd, pp. 1–24, 1999.

[11] J. Ainslie, "Calculating the flowfield in the wake of wind turbines", *Journal of Wind Engineering and Industrial Aerodynamics*, vol. 27th, pp. 213–224, 1988.

[12] D. R. VanLuvanee, "Investigation of observed and modeled wake effects at horns rev using windpro", Master's thesis, Technical University of Denmark, 2006.

[13] A. Zhang J Messac and et all, "Impact of different wake models on the estimation of wind farm power generation", AIAA/ISSMO Multidisciplinary Analysis and Optimization Conference, vol. 14th, 2012.

[14] S. Frandsen, M. Thøgersen, and et all, "Analytical modelling of wind speed deficit in large offshore wind farms", *Wind energy*, vol. 9th, pp. 39–53, 2006.

[15] T. Ishihara, A. Yamaguchi, and Y. Fujino, "Development of a new wake model based on a wind tunnel experiment", *Tech. rep., Global Wind*, 2004.

[16] A. Crespo and J. Hernandez, "Turbulence characteristics in wind turbine wakes", *Journal of Wind Engineering and Industrial Aerodynamics*, vol. 61th, pp. 71–85, 1996.

[17] D. Quarton, "Characterization of wind turbine wake turbulence and its implications on wind farm spacing", *Department of Energy of the UK*, vol. Final Report ETSU WN 5096, 1989.

[18] S. Frandsen and M. Thøgersen, "Integrated fatigue loading for wind turbines in wind farms by combining ambient turbulence and wakes.", *Wind Eng*, vol. 23th, pp. 327–40, 199.

[19] P. Å. Krogstad and J. Lund, "An experimental and numerical study of the performance of a model turbine", *Wind Energy*, vol. 15th, pp. 443–457, 2012.

[20] O. De Vries, "On the theory of the horizontal-axis wind turbine", *Ann Rev Fluid Mech*, vol. 15th, pp. 77–96, 1983.

[21] A. Dantec Dynamics, "Ldv diagram", *Nova Instruments Company*, 2017.

[22] F. Pierella and L. Sætran, "Wind tunnel investigation on the effect of the turbine tower on wind turbines wake symmetry",

[23] S. J, O. T. S. G, and P. J, "Analysis of wake measurements form the ecn wind turbine test site wieringemeer ewtw", *Wind Energy*, vol. 15, p. 575, 2012.

[24] C. Helmis, P. Papageorgas, and et all, "An experimental study of the near wake structure of a wind turbine operating over complex terrain", *Solar Energy*, vol. 54th, pp. 413–428, 1995.

Appendix A

Experimental results

A.1 Lines drag disk with grid

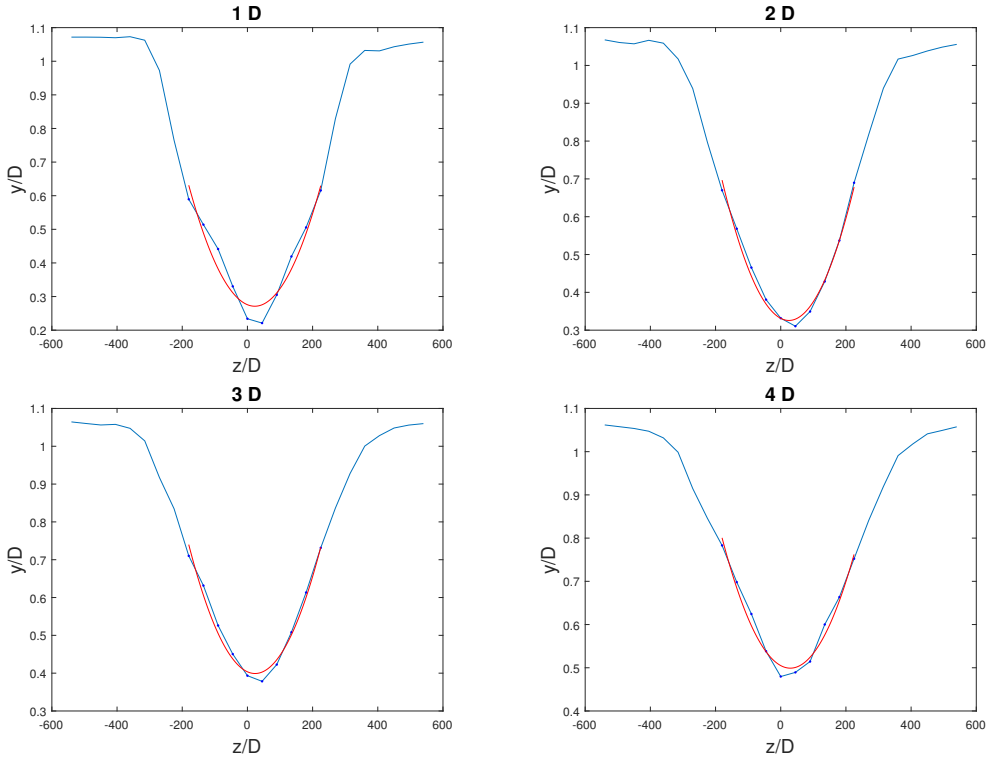

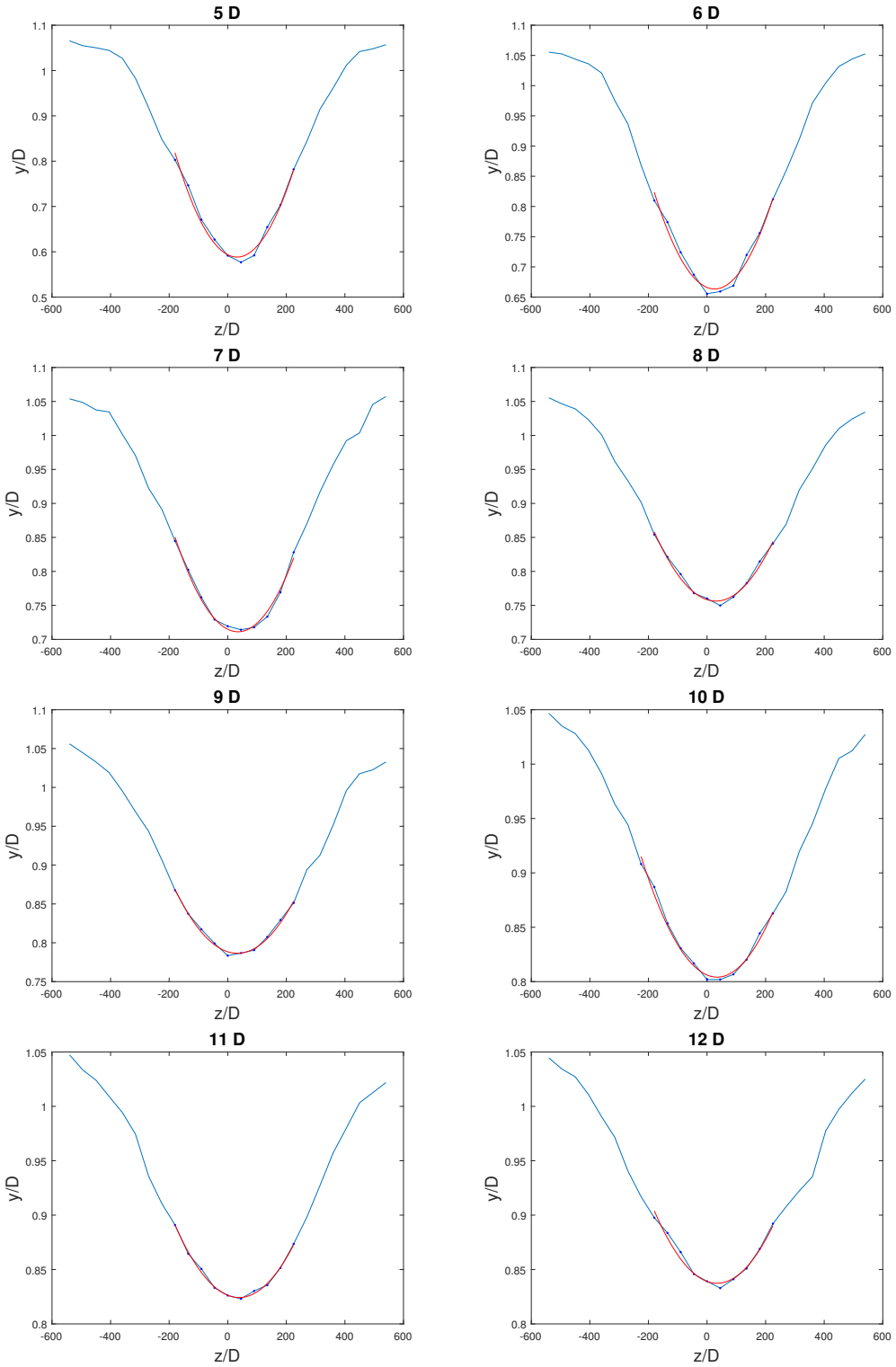
5 D
6 D
7 D
8 D
9 D
10 D
11 D
12 D
y/D
z/D

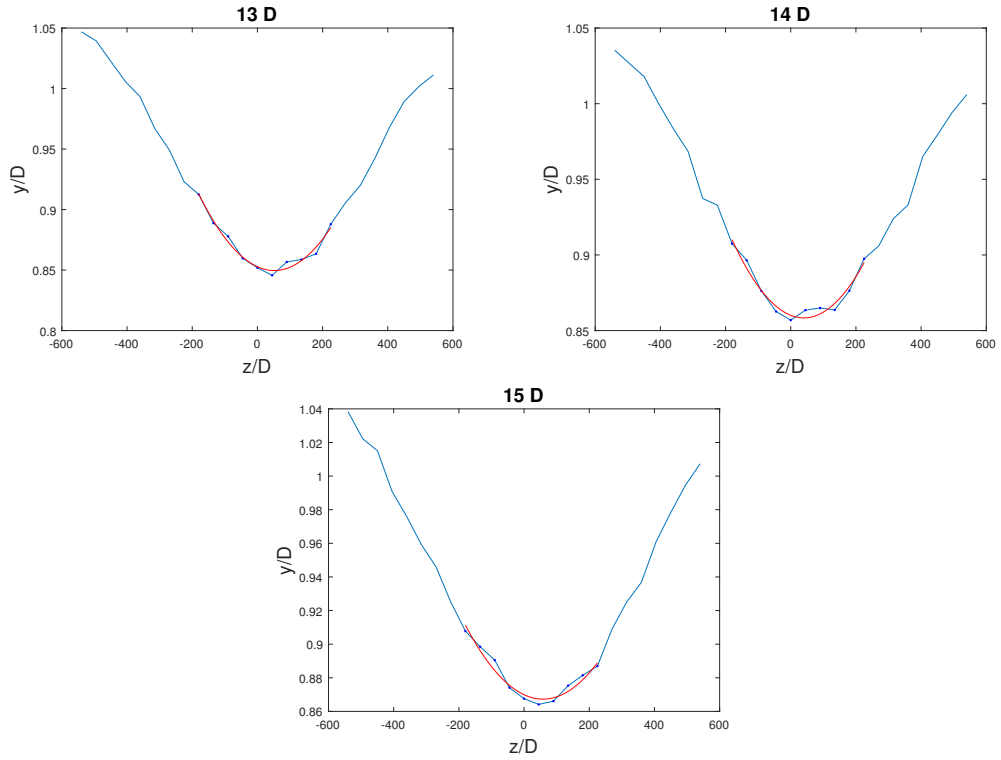

A.2 Lines drag disk without grid

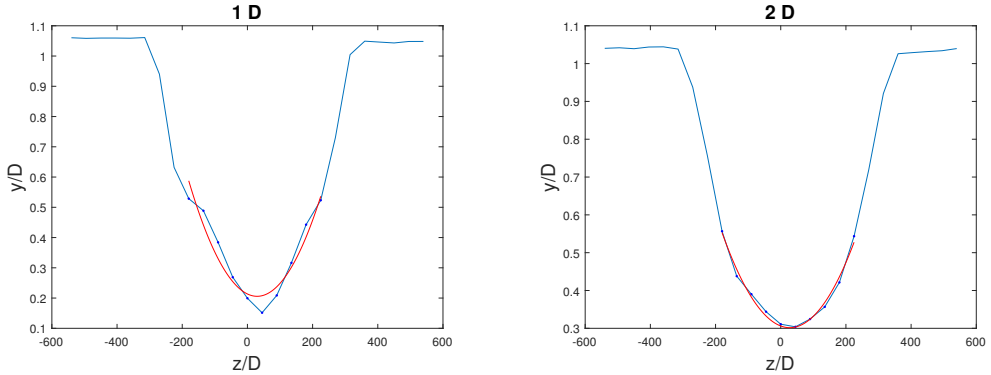

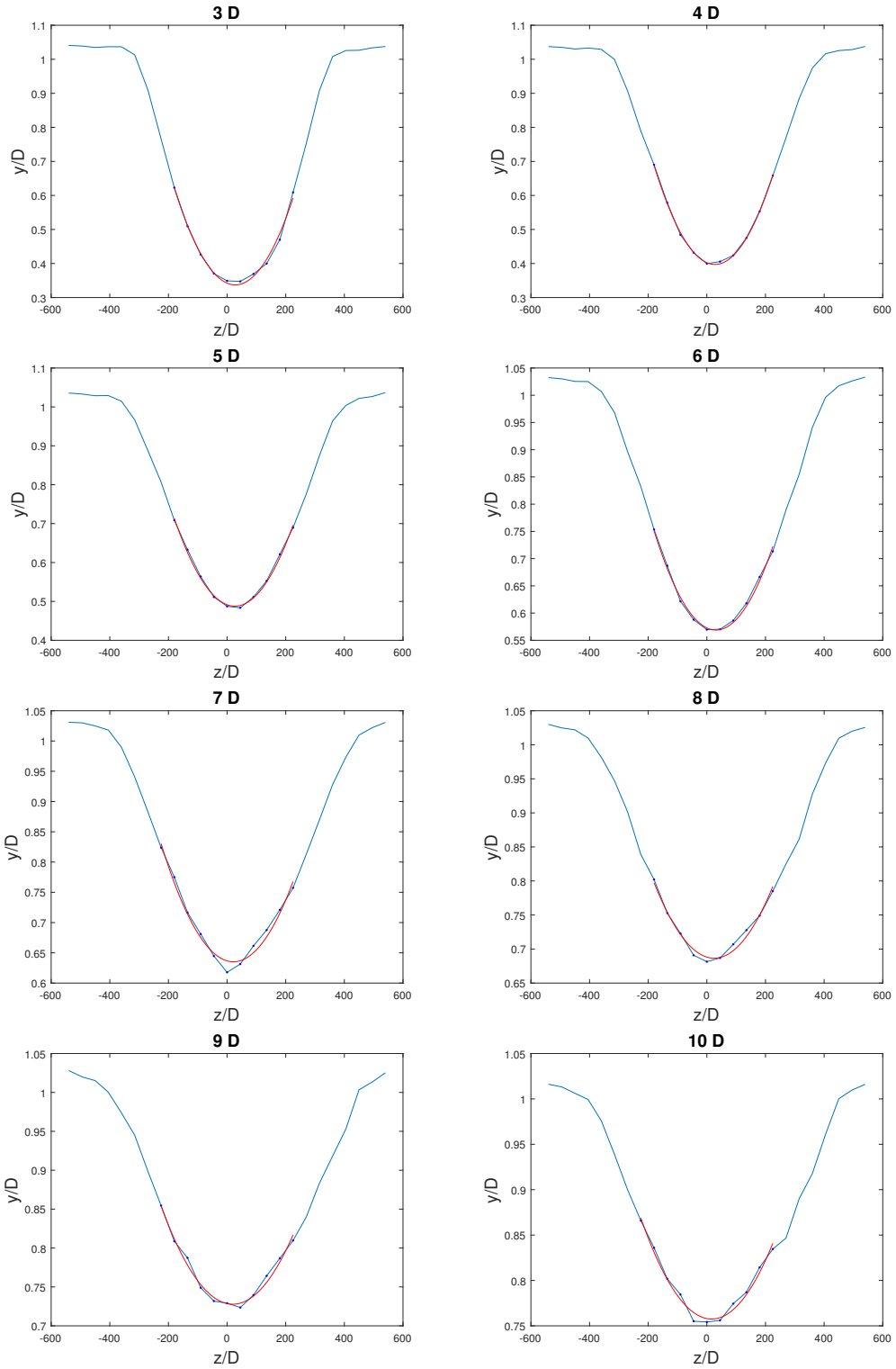
3 D
4 D
5 D
6 D
7 D
8 D
9 D
10 D
y/D
z/D

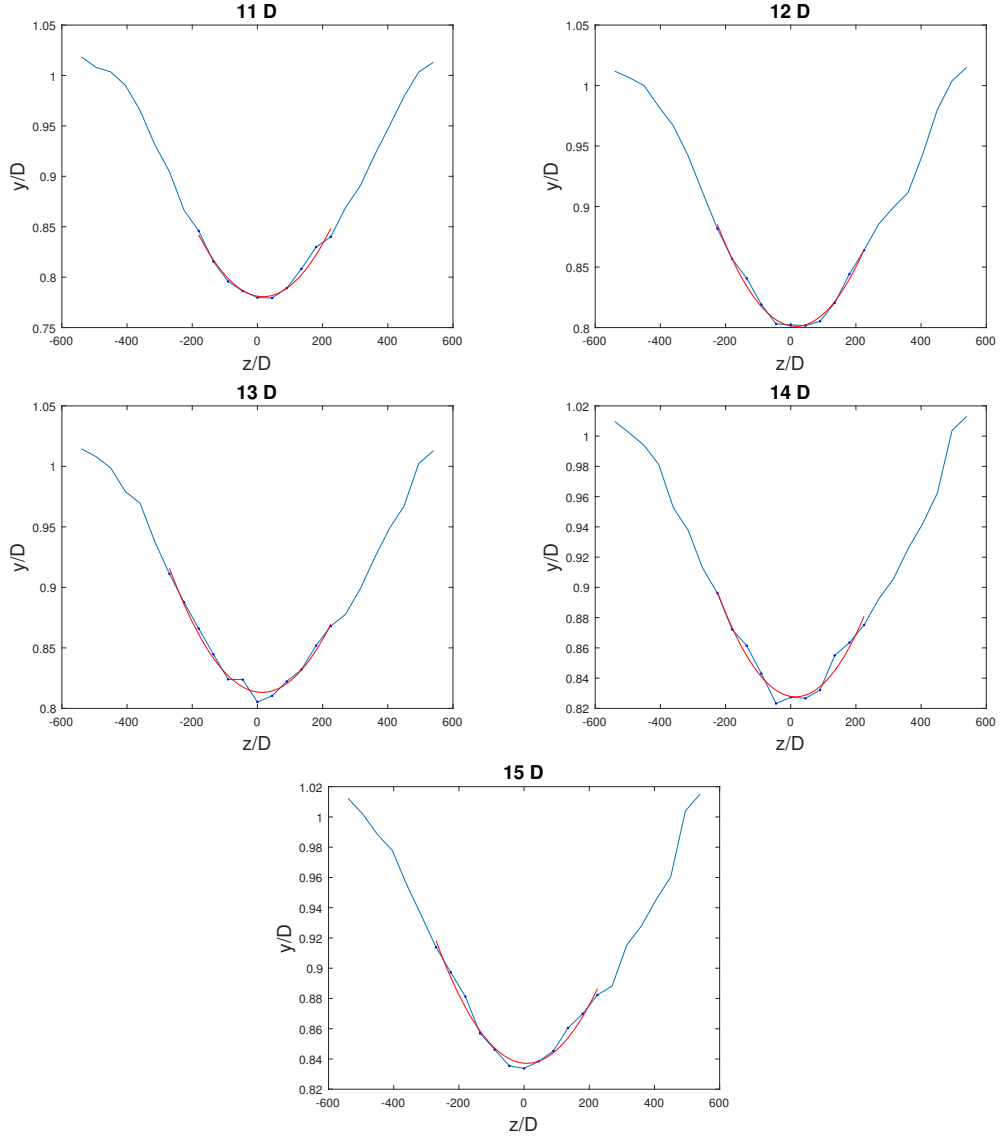
11 D
12 D
13 D
14 D
15 D
y/D
z/D

A.3 Lines wind turbine with grid

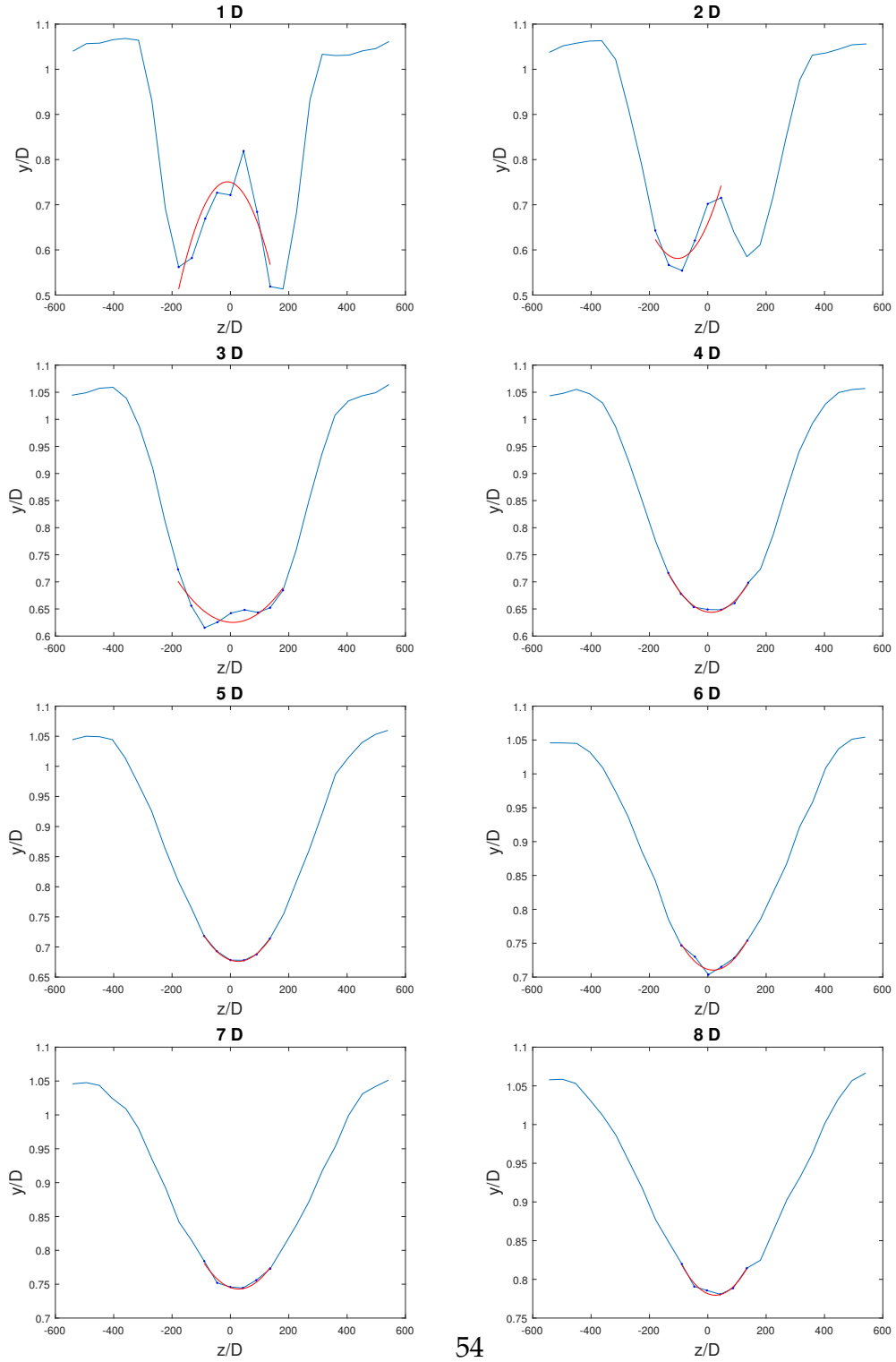

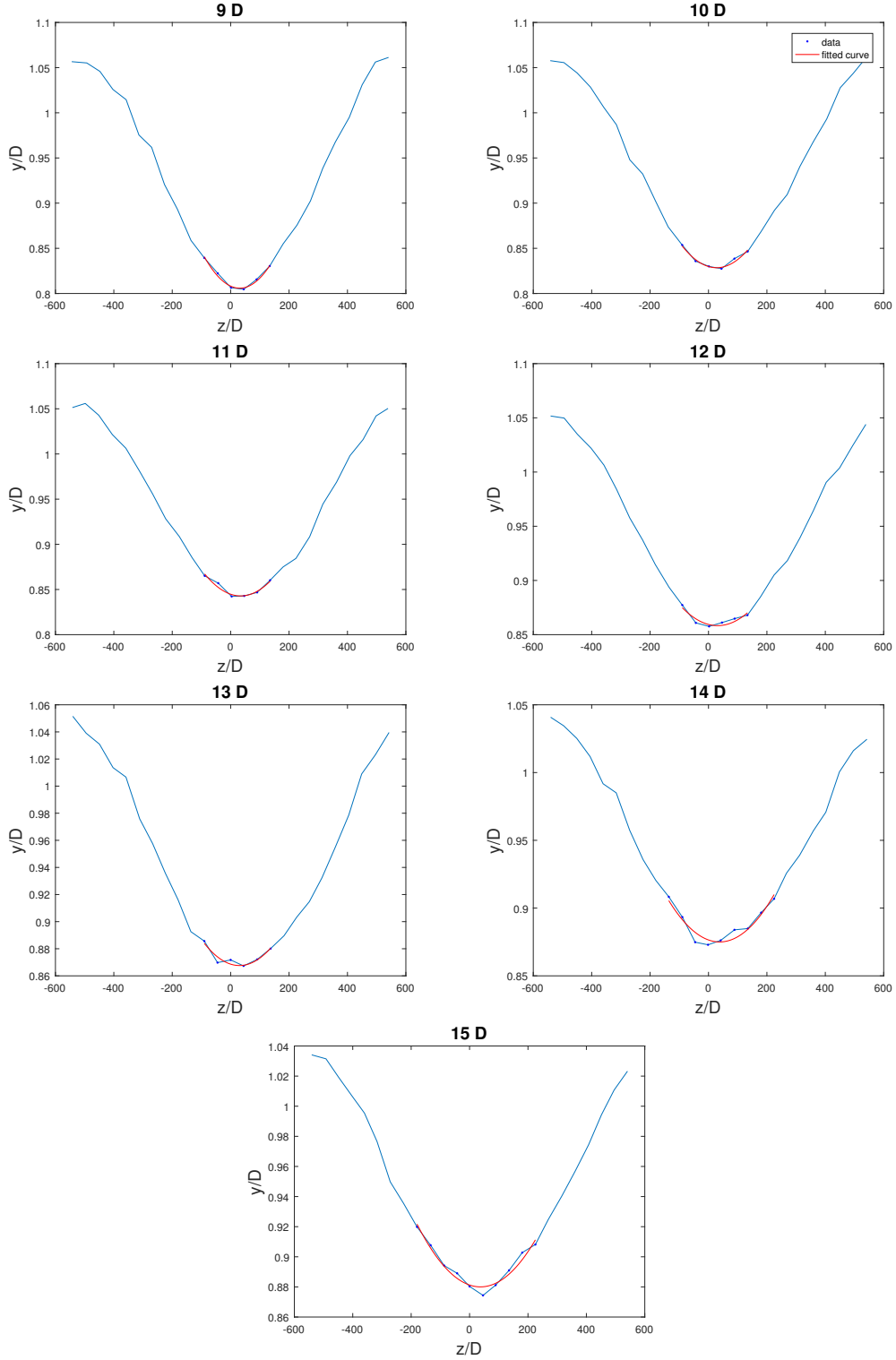
9 D
10 D
data
fitted curve
11 D
12 D
13 D
14 D
15 D
y/D
z/D

A.4 Lines wind turbine without grid

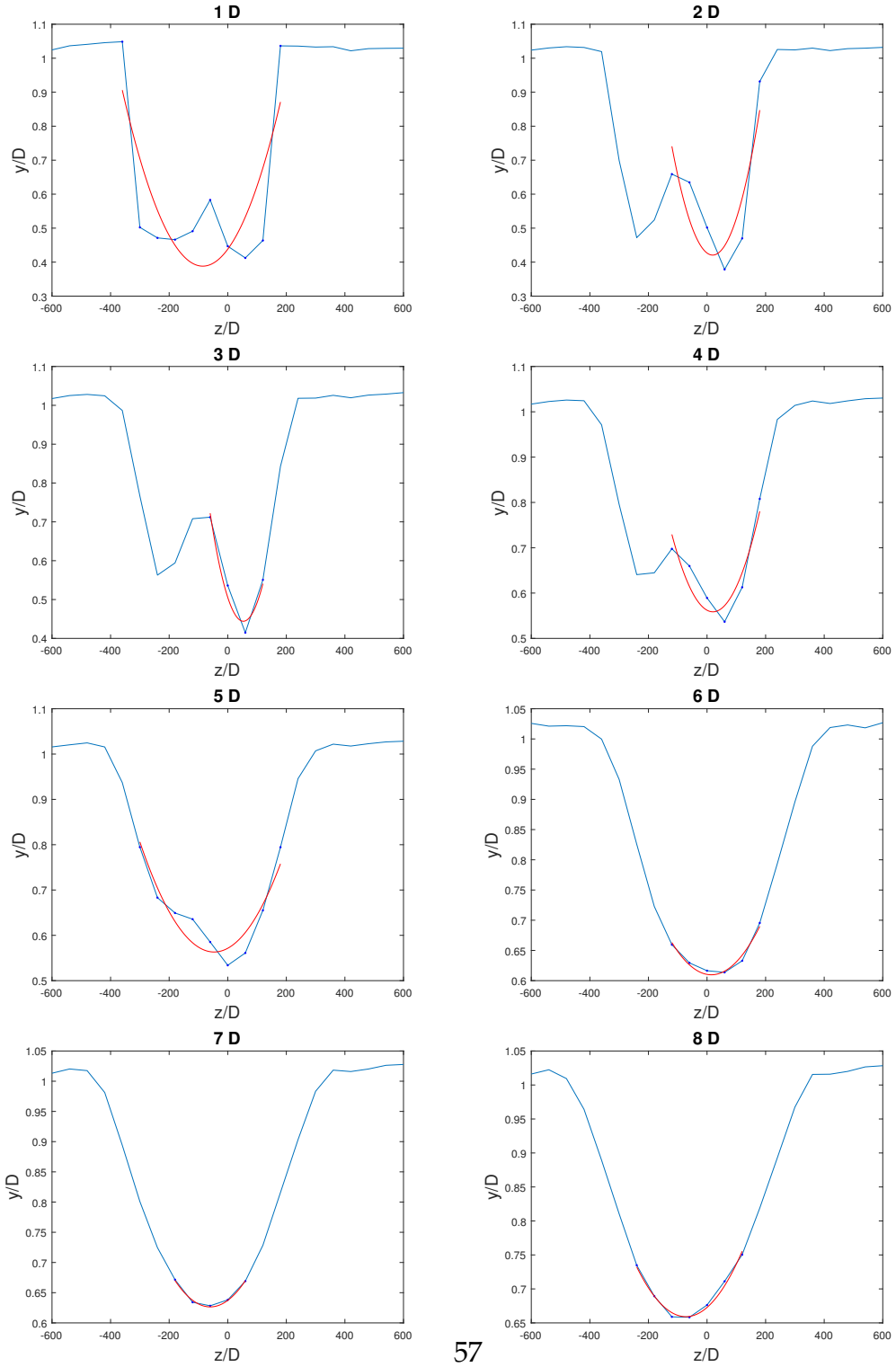

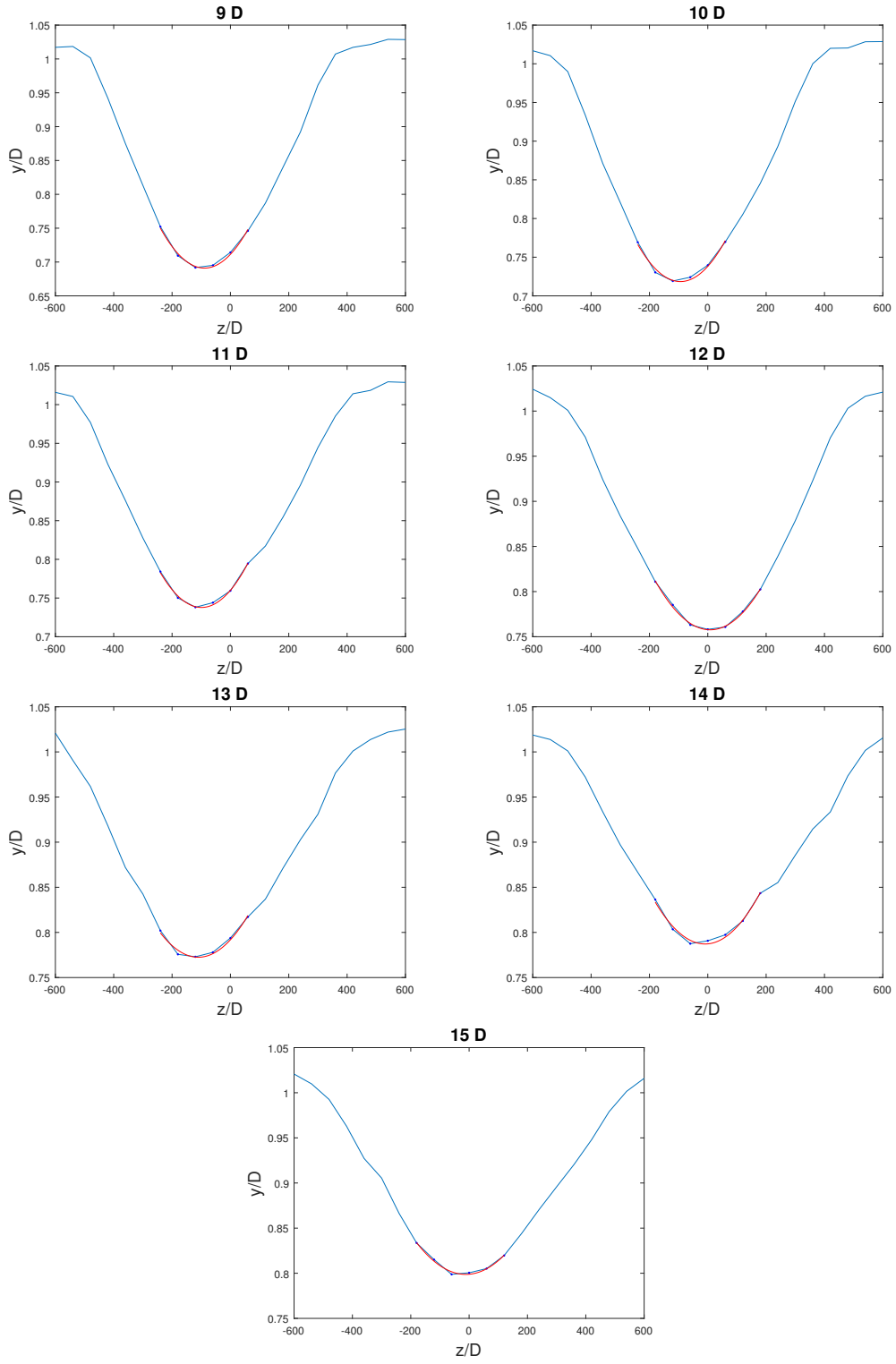
9 D
10 D
11 D
12 D
13 D
14 D
15 D
y/D
z/D